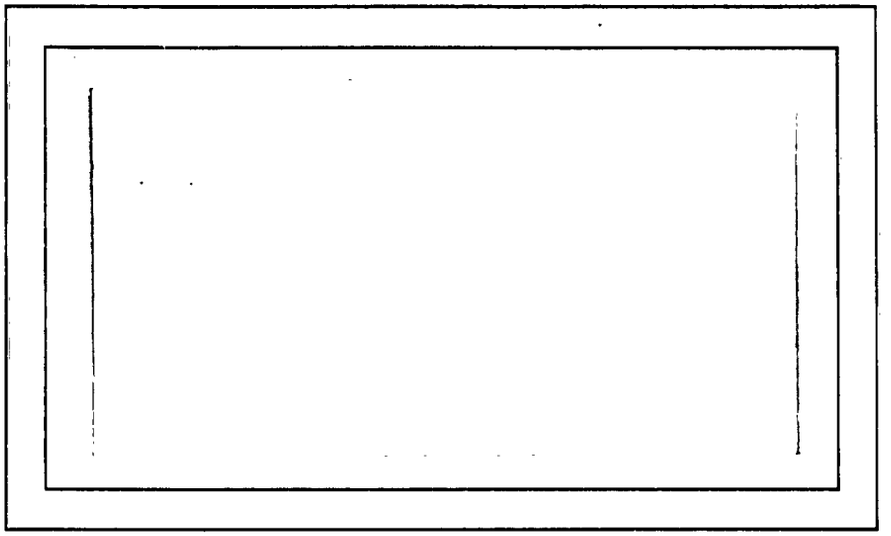

THERM ADVANCED RESEARCH
DIVISION OF
THERM
Incorporated
ITHACA, NEW YORK

THE AERODYNAMIC LOADING ON STREAMLINED DUCTED BODIES

by

Gary R. Hough

TAR-TR 625 December 1962

Submitted to Air Programs, Office of Naval Research in partial fulfillment of Contract Nonr-2859(00)

Donald Earl Ordway
Donald Earl Ordway
Head, Aerophysics Section

Approved:

A. Ritter
A. Ritter
Director, Therm Advanced Research

ACKNOWLEDGMENT

The author wishes to extend his sincere appreciation to Dr. D. E. Ordway for his many helpful suggestions; to Messrs. C. F. Lo and A. L. Kaskel for checking the equations and numerical calculations; and to Mrs. Sally Jack of the Cornell University Computing Center for programming and carrying out the necessary computer operations.

ABSTRACT

A simple method for the rapid determination of the linearized surface pressure distribution on streamlined ducted bodies in axisymmetric flow is developed using conventional singularity distributions. The final form of the pressure coefficient is expressed directly as a single matrix operation on the duct sectional properties and tables of the necessary matrix coefficients are given. Several numerical examples are worked out and compared with the results of previous theoretical and experimental investigations.

TABLE OF CONTENTS

PRINCIPAL NOMENCLATURE

a_n	coefficients of source distribution expansion related to A_n by Eqs. (2.6)
A_n	coefficients of thickness distribution expansion
c	duct chord
c_m	duct sectional pitching moment coefficient
c_p	duct surface pressure coefficient
c_r	duct sectional radial force coefficient
c_ν	coefficients of Glauert series for γ
$c_\nu^{2\text{-D}}$	two-dimensional Glauert coefficients
C	non-dimensional duct vortex distribution, γ/U
f	strength per unit length of bound duct sources
F	pressure coefficient of two-dimensional airfoil with thickness t and no camber
$h_{p,q}$	coefficients of Fourier series expansion for $\mathcal{R}_1$
I_1	$\frac{1}{2\pi}\{Q'_{\frac{1}{2}}(\tilde{\omega}) - Q'_{-\frac{1}{2}}(\tilde{\omega})\}$
I_2	$\frac{1}{2\pi}\,\Delta\bar{x}\,Q'_{-\frac{1}{2}}(\tilde{\omega})$
$j_{p,q}$	coefficients of Fourier series expansion for $\mathcal{R}_2$

p	static pressure
$Q_{\frac{1}{2}}(\omega)$	Legendre function of second kind and plus one-half order
$Q_{-\frac{1}{2}}(\omega)$	Legendre function of second kind and minus one-half order
r	radial coordinate
R	duct reference radius
$\mathcal{R}_1$	regular part of I_1
$\mathcal{R}_2$	regular part of I_2
t	duct thickness distribution
u_f	axial velocity induced by bound ring sources
u_γ	axial velocity induced by bound ring vortices
U	free stream velocity
v_f	radial velocity induced by bound ring sources
v_γ	radial velocity induced by bound ring vortices
x	axial coordinate
γ	strength per unit length of bound duct vortices
$\Delta\bar{x}$	$\bar{x} - \bar{\xi}$

ϵ	inclination of duct camber line relative to x axis
ϵ_e	duct effective camber, $\epsilon_e \equiv \epsilon - \epsilon_t$
ϵ_t	thickness-induced camber
θ	circumferential coordinate
λ	c/2R
ξ	axial variable
ϕ	angular variable, $\bar{x} = -\lambda \cos \phi$
Φ	velocity potential for isolated source ring
φ	angular variable, $\bar{\xi} = -\lambda \cos \varphi$
Ψ	stream function for isolated vortex ring
ϖ	argument of Legendre functions
$\tilde{\varpi}$	$1 + \frac{\Delta\bar{x}^2}{2}$
$(\bar{})$	quantity nondimensionalized with respect to R ; e. g., $\bar{x} \equiv x/R$
$(')$	differentiation of a function with respect to its indicated argument
$[\ ]$	infinite column matrix
$[\ ]$	infinite square matrix

THE AERODYNAMIC LOADING ON STREAMLINED DUCTED BODIES

INTRODUCTION

During the past three years we have formulated[1] and studied[2,3] a three-dimensional theory for the finite-bladed shrouded propeller in the forward flight regime. The mathematical model chosen to represent the system was based on the classical concepts of vortex propeller theory and of lifting-surface theory for ring wings of zero thickness in inviscid, incompressible flow. The purpose of this report is to remove the limitation of zero thickness as all shrouds have a finite thickness which may contribute substantially to the determination of such quantities as the shroud loading and propeller inflow. Since the effect of the propeller may be simply superimposed within the framework of linearized theory, it is sufficient for our purposes to limit our attention directly to the problem of the annular airfoil.

The problem of finding the detailed velocity field associated with and the forces acting on annular airfoils in incompressible flow has been the subject of extensive investigation over the past twenty-five years. Possibly the earliest treatment using singularity distributions and classical thin-airfoil theory was given by H. E. Dickmann[4] in 1940. Since that time, many contributions[5-12] have appeared, culminating in the studies[13-19]

of J. Weissinger, who was the first to give a comprehensive treatment of the thickness problem. Nevertheless, in spite of all the work which has been undertaken, a simple, accurate method had not yet been developed for the rapid prediction of duct surface pressure distributions for preliminary design studies.

In this report, such a method for the linearized pressure distribution in the case of axisymmetric flow is developed. The results obtained are presented in a form such that they may be incorporated directly into our previous studies of the ducted propeller or used "as is" in the treatment of ducted bodies.

The conventional mathematical model of ring vortices and sources distributed on a reference cylinder is chosen to represent the duct and the approximations of thin-airfoil theory are employed throughout. The source strength depends only upon the rate of change of the airfoil profile thickness. In turn, this distribution induces a radial wash which, together with that induced by the vortex distribution, must be equal to the local camber everywhere on the duct surface. With the thickness distribution given in a generalized form of the NACA four-and five-digit airfoil series, the thickness-induced radial wash is expressed in appropriate matrix form. The solution for the unknown vortex strength follows immediately using the iteration technique of D. E. Ordway and M. D. Greenberg[2]. Then the linearized surface pressure distribution is reduced to a single matrix operation on the duct sectional properties. The effect

of the duct chord-to-diameter ratio is explicitly obtained and tables of all necessary matrix coefficients are given for four typical values of this parameter. Incidentally, several definite integrals not appearing in common integral tables[20,21] were evaluated during the course of this work and have been collected in an appendix.

Briefly, the report is presented as follows. The first Chapter gives the mathematical formulation of the problem, the derivation of the induced velocity field, and the procedure for finding the strengths of the source and vortex distributions. Chapter Two details the reduction of the thickness-induced radial wash to matrix form in terms of the known thickness distribution coefficients. In Chapter Three, the duct surface coefficient is found in matrix form and simple expressions for the sectional radial force and pitching moment coefficients are furnished. Tabulated values of all the required matrix coefficients for four body chord-to-diameter ratios are presented. Several numerical examples are worked out to illustrate the computational technique and to compare with previous theoretical and experimental results in Chapter Four.

CHAPTER ONE

BASIC FORMULATION

1.1 Mathematical Model

Consider an annular airfoil, or duct, at zero incidence in a uniform, inviscid, incompressible stream U, see Fig. 1.1. A cylindrical coordinate system (x,r,θ) is chosen with the origin fixed at the center of the duct, $x = -c/2$ corresponding to the duct leading edge and $x = +c/2$ to the trailing edge. The duct section is assumed known and is the same at every azimuthal station. The local inclination of the camber line to the x-axis is denoted by $\epsilon(x)$ and the thickness distribution by $t(x)$. Both ϵ and t/c are assumed small.

Making the conventional approximations of linearized perturbations, the annular airfoil is replaced by a distribution of ring sources and vortices on an appropriate reference cylinder of radius R. Due to the axisymmetry of the flow field, the source strength per unit length f does not vary with θ. The same is true of the vortex strength per unit length γ. Since $\gamma = \gamma(x)$, there are no trailing vortices from the duct.

The strength of these distributions will be determined from the physical boundary condition that the flow be everywhere tangent to the duct surface together with the Kutta-Joukowski condition at the trailing edge. Consistent with our assumptions,

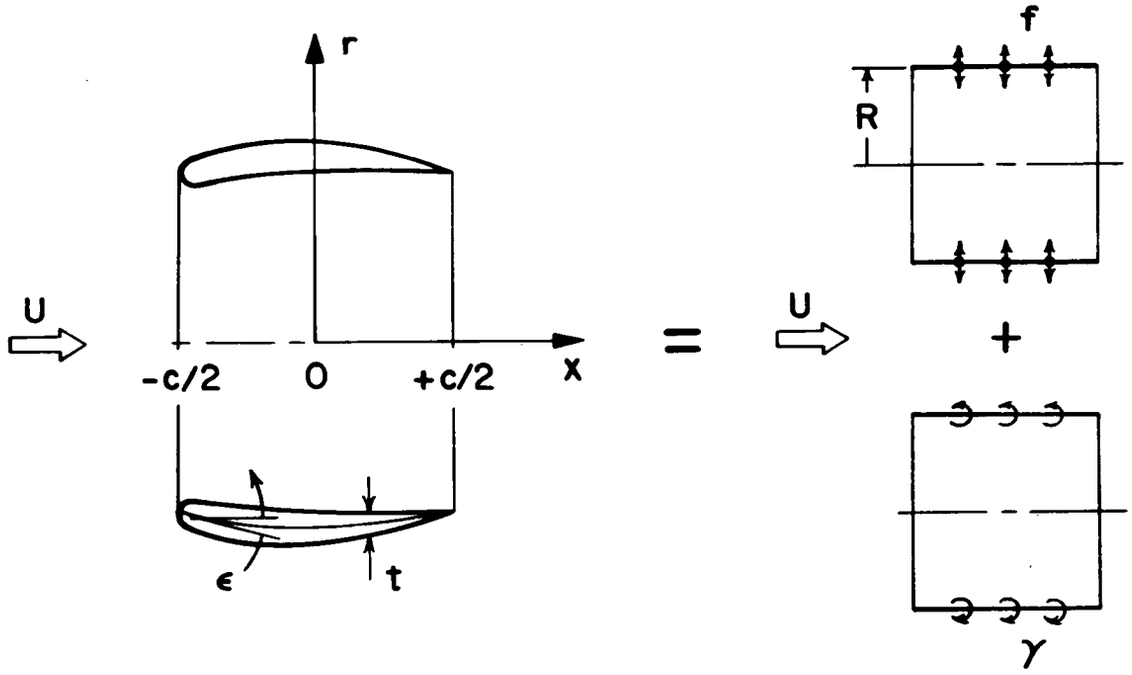

FIGURE 1.1

ANNULAR AIRFOIL GEOMETRY AND
EQUIVALENT SINGULARITY DISTRIBUTIONS

this reduces to the familiar thin-airfoil approximation

$$\epsilon \pm \frac{1}{2} t' = \frac{v_f + v_\gamma}{U} \tag{1.1}$$

where v_f and v_γ are the radial velocities induced on the reference cylinder by the source and vortex distributions respectively and $\gamma(c/2) = 0$. Throughout the report we adopt the convention that the prime ($'$) denotes total differentiation of a function with respect to its indicated argument and, in the event a double sign precedes a quantity, the top sign is to be used to give the value on the outer duct surface and the bottom sign, the value on the inner surface.

1.2 Induced Velocity Field

To solve Eq. (1.1) the radial component of the velocities induced by f and γ are required. Subsequently, the axial component will be needed for the pressure coefficient. Therefore, we will derive general expressions for both before we proceed.

The velocity potential Φ for an isolated source ring of unit strength is generally expressed in terms of the complete elliptic integral of the first kind. Alternatively, we may use the relation[22] between this function and the Legendre function of second kind and minus one-half order $Q_{-\frac{1}{2}}(\omega)$ to obtain,

$$\Phi = -\frac{1}{2\pi R}\,\frac{1}{\sqrt{\bar{r}}}\,Q_{-\frac{1}{2}}(\omega)$$

$$\omega \equiv 1 + \frac{\Delta\bar{x}^2 + (\bar{r}-1)^2}{2\bar{r}} \tag{1.2}$$

where $x/R \equiv \bar{x}$, $r/R \equiv \bar{r}$, ... and $\Delta\bar{x}$ is the axial separation of the field point and the singularity at $\bar{\xi}$, $\Delta\bar{x} \equiv \bar{x} - \bar{\xi}$. The corresponding axial and radial velocities are gotten from $\partial\Phi/\partial x$ and $\partial\Phi/\partial r$ respectively. Upon reduction of the latter velocity by recursion relations[22] and chordwise integration of both over f , we find for the resultant contribution u_f to the axial perturbation velocity,

$$u_f(\bar{x},\bar{r}) = \frac{-1}{2\pi\bar{r}^{3/2}} \int_{-\lambda}^{\lambda} f(\bar{\xi})\,\Delta\bar{x}\,Q'_{-\frac{1}{2}}(\omega)\,d\bar{\xi} \tag{1.3}$$

and v_f to the radial perturbation velocity,

$$v_f(\bar{x},\bar{r}) = \frac{1}{2\pi\bar{r}^{3/2}} \int_{-\lambda}^{\lambda} f(\bar{\xi})\,\{Q'_{\frac{1}{2}}(\omega) - \bar{r}Q'_{-\frac{1}{2}}(\omega)\}\,d\bar{\xi} \tag{1.4}$$

where $\lambda \equiv c/2R$ and $Q_{\frac{1}{2}}(\omega)$ is the Legendre function of second kind and plus one-half order.

On the other hand, the velocity components for an isolated vortex ring of unit strength may be found most easily from the stream function Ψ . In terms of $Q_{\frac{1}{2}}(\omega)$, we have[23] ,

$$\Psi = \frac{R}{2\pi}\,\sqrt{\bar{r}}\,Q_{\frac{1}{2}}(\omega) \tag{1.5}$$

with ω as defined in Eq. (1.2). The corresponding axial and radial velocities are gotten from $(1/r)\,\partial\Psi/\partial r$ and $(-1/r)\,\partial\Psi/\partial x$ respectively. After reduction of the former velocity by recursion relations[22] and chordwise integration of both over γ, we get for the axial component u_γ,

$$u_\gamma(\bar{x},\bar{r}) = \frac{1}{2\pi\bar{r}^{3/2}} \int_{-\lambda}^{\lambda} \gamma(\bar{\xi}) \{\bar{r}Q'_{\frac{1}{2}}(\omega) - Q'_{-\frac{1}{2}}(\omega)\}\, d\bar{\xi} \tag{1.6}$$

and the radial component v_γ,

$$v_\gamma(\bar{x},\bar{r}) = \frac{-1}{2\pi\bar{r}^{3/2}} \int_{-\lambda}^{\lambda} \gamma(\bar{\xi})\, \Delta\bar{x}\, Q'_{\frac{1}{2}}(\omega)\, d\bar{\xi} \tag{1.7}$$

To evaluate u_f, v_f, u_γ and v_γ on the reference cylinder, or $\bar{r} = 1$, we follow the usual procedures of thin-airfoil theory. This has been previously carried out in detail in terms of the associated elliptic functions[10] and has been repeated using the small argument expansion[22] of $Q_{\frac{1}{2}}$ and $Q_{-\frac{1}{2}}$, yielding

$$u_f(\bar{x},1) = -\frac{1}{2\pi} \int_{-\lambda}^{\lambda} f(\bar{\xi})\, \Delta\bar{x}\, Q'_{-\frac{1}{2}}(\tilde{\omega})\, d\bar{\xi} \tag{1.8}$$

$$v_f(\bar{x},1) = \pm\frac{1}{2} f(\bar{x}) + \frac{1}{2\pi} \int_{-\lambda}^{\lambda} f(\bar{\xi}) \{Q'_{\frac{1}{2}}(\tilde{\omega}) - Q'_{-\frac{1}{2}}(\tilde{\omega})\}\, d\bar{\xi} \tag{1.9}$$

$$u_\gamma(\bar{x},1) = \mp\frac{1}{2} \gamma(\bar{x}) + \frac{1}{2\pi} \int_{-\lambda}^{\lambda} \gamma(\bar{\xi}) \{Q'_{\frac{1}{2}}(\tilde{\omega}) - Q'_{-\frac{1}{2}}(\tilde{\omega})\}\, d\bar{\xi} \tag{1.10}$$

$$v_\gamma(\bar{x},1) = -\frac{1}{2\pi}\int_{-\lambda}^{\lambda} \gamma(\bar{\xi})\ \Delta\bar{x}\ Q'_{\frac{1}{2}}(\tilde{\varpi})\ d\bar{\xi} \tag{1.11}$$

where

$$\tilde{\varpi} \equiv 1 + \frac{\Delta\bar{x}^2}{2} \tag{1.12}$$

1.3 Determination of Source and Vortex Strengths

Formally, f and γ are coupled by Eq. (1.1). However, from Eqs. (1.9) and (1.11), only v_f and not v_γ is discontinuous across the reference cylinder. Thus we must have

$$f(\bar{x}) = Ut'(\bar{x}) \tag{1.13}$$

and the required source strength depends only upon the rate of change of the duct thickness distribution as for the problem of the two-dimensional airfoil[10].

Consequently, with f determined we may regard the continuous part of v_f as a <u>thickness-induced camber</u> ϵ_t defined by

$$\epsilon_t \equiv \frac{1}{2\pi}\int_{-\lambda}^{\lambda} t'(\bar{\xi})\ \{Q'_{\frac{1}{2}}(\tilde{\varpi}) - Q'_{-\frac{1}{2}}(\tilde{\varpi})\}\ d\bar{\xi} \tag{1.14}$$

and combined with ϵ to form an <u>effective camber</u> ϵ_e,

$$\epsilon_e \equiv \epsilon - \epsilon_t \tag{1.15}$$

Then Eq. (1.1) can be rewritten as

$$\epsilon_e = -\frac{1}{2\pi}\int_{-\lambda}^{\lambda} C(\bar{\xi})\,\Delta\bar{x}\,Q_{\frac{1}{2}}'(\tilde{\omega})\,d\bar{\xi} \tag{1.16}$$

where

$$\gamma \equiv UC(\bar{x}) \tag{1.17}$$

Eq. (1.16) constitutes an integral equation for the unknown vortex distribution C. To solve, we shall use the iterative procedure of Ordway and Greenberg. A new axial coordinate ϕ is introduced such that

$$\bar{x} = -\lambda\,\cos\phi \tag{1.18}$$

where $0 \leq \phi \leq \pi$ and C is expressed in a Glauert series,

$$C = c_0 \cot\frac{\phi}{2} + \sum_{\nu=1}^{\infty} c_\nu \sin\nu\phi \tag{1.19}$$

Such a series satisfies the Kutta-Joukowski condition at the trailing edge and possesses the proper square-root singularity at the leading edge in the cotangent term. The corresponding Glauert coefficients are then given in matrix form[2] as

$$\{c\} = ([I] + [P] + [P]^2 + [P]^3 + \ldots)\{c^{2-D}\} \tag{1.20}$$

where

$$\{c\} \equiv \begin{Bmatrix} c_0 \\ c_1 \\ c_2 \\ \cdot \\ \cdot \\ \cdot \end{Bmatrix} \tag{1.21}$$

and $\{c^{2-D}\}$ is a column matrix of the Glauert coefficients of a two-dimensional airfoil having a camber equal to ϵ_e, these coefficients being given by,

$$c_0^{2-D} = \frac{2}{\pi} \int_0^{\pi} \epsilon_e \, d\phi$$

$$c_\nu^{2-D} = -\frac{4}{\pi} \int_0^{\pi} \epsilon_e \cos \nu\phi \, d\phi \qquad \nu \geq 1 \tag{1.22}$$

$[I]$ is the unit matrix and $[P]$ is a square matrix whose coefficients are functions only of λ. Each term of the operator $([I] + [P] + [P]^2 + \ldots)$ corresponds to a step in the iteration process which in the limit converges to the exact solution, cf. Ref. 13. The leading forty-nine elements of $[P]$ are given in Ref. 2 for $\lambda = 1/4, 1/2, 3/4$ and 1 which covers the range of practical interest. For convenience, we have computed the elements of $([I] + [P] + [P]^2 + \ldots)$ for these λ to an

accuracy of $\pm 1 \times 10^{-4}$. These are presented in Tables 1.1-1.4. Since the elements diminish rapidly off the diagonal and approach unity quickly on the diagonal, engineering accuracy can be achieved in a few steps. Of course as the chord-to-diameter ratio increases, the three-dimensional effect increases and the speed of convergence decreases.

In summary, the source strength is found immediately from the known thickness distribution, see Eq. (1.13), and so ϵ_t . From ϵ_t and ϵ , the Glauert coefficients of the vortex distribution are then found from a single matrix operation on the corresponding coefficients of Eqs. (1.22) for a two-dimensional airfoil with camber ϵ_e .

1.0277	0	0.0139	0	0.0000	0	0.0000
0.0568	1.0308	0.0008	-0.0031	0.0000	0.0000	0.0000
0.0063	0	1.0041	0	-0.0010	0	0.0000
-0.0001	-0.0010	0.0000	1.0015	0.0000	-0.0005	0.0000
0.0000	0	-0.0005	0	1.0008	0	-0.0003
0.0000	0.0000	0.0000	-0.0003	0.0000	1.0005	0.0000
0.0000	0	0.0000	0	-0.0002	0	1.0003

TABLE 1.1

ELEMENTS OF $([I] + [P] + [P]^2 + \ldots)$ **FOR** $\lambda = 1/4$

1.0796	0	0.0400	0	-0.0002	0	0.0000
0.1719	1.0933	0.0064	-0.0138	0.0000	0.0001	0.0000
0.0274	0	1.0179	0	-0.0042	0	0.0000
-0.0009	-0.0046	0.0000	1.0062	0.0000	-0.0020	0.0000
-0.0002	0	-0.0021	0	1.0032	0	-0.0012
0.0000	0.0000	0.0000	-0.0012	0.0000	1.0020	0.0000
0.0000	0	0.0000	0	-0.0008	0	1.0013

TABLE 1.2

ELEMENTS OF $([I] + [P] + [P]^2 + \ldots)$ **FOR** $\lambda = 1/2$

1.1398	0	0.0704	0	-0.0005	0	0.0000
0.3186	1.1722	0.0197	-0.0329	-0.0001	0.0004	0.0000
0.0650	0	1.0425	0	-0.0101	0	0.0001
-0.0022	-0.0110	-0.0001	1.0147	0.0000	-0.0047	0.0000
-0.0008	0	-0.0051	0	1.0074	0	-0.0028
0.0000	0.0001	0.0000	-0.0028	0.0000	1.0045	0.0000
0.0000	0	0.0000	0	-0.0018	0	1.0031

TABLE 1.3

ELEMENTS OF $([I] + [P] + [P]^2 + \ldots)$ **FOR** $\lambda = 3/4$

1.2018	0	0.1015	0	0.0001	0	-0.0001
0.4850	1.2608	0.0410	-0.0599	-0.0002	0.0010	0.0000
0.1179	0	1.0778	0	-0.0192	0	0.0003
-0.0027	-0.0200	-0.0002	1.0276	0.0000	-0.0089	0.0000
-0.0019	0	-0.0097	0	1.0138	0	-0.0051
-0.0003	0.0002	0.0000	-0.0053	0.0000	1.0083	0.0000
0.0000	0	0.0001	0	-0.0034	0	1.0056

TABLE 1.4

ELEMENTS OF $([I] + [P] + [P]^2 + \ldots)$ **FOR** $\lambda = 1$

CHAPTER TWO

REDUCTION OF EFFECTIVE CAMBER

2.1 General Considerations

From Eqs. (1.22) we see that the determination of the two-dimensional Glauert coefficients is equivalent to decomposing ϵ_e into the Fourier cosine series

$$\epsilon_e = \frac{1}{2}\epsilon_{e_0} - \frac{1}{2}\sum_{\nu=1}^{\infty} \epsilon_{e_\nu} \cos \nu\phi \tag{2.1}$$

i. e.,

$$\{c^{2-D}\} = \{\epsilon_e\} \equiv \{\epsilon\} - \{\epsilon_t\} \tag{2.2}$$

We will assume that $\{\epsilon\}$ or the contribution of the geometrical camber to $\{\epsilon_e\}$ is known by evaluation of Eqs. (1.22) with ϵ_e replaced by ϵ, cf. Ref. 24, or by direct expression of ϵ in the form of Eq. (2.1), cf. Ref. 25. The contribution $\{\epsilon_t\}$ of the thickness-induced camber will now be determined. To carry this out, t' and the second factor in the integrand of Eq. (1.14), say I_1, are expressed in forms suitable for integration. We find each of these is composed of a singular as well as a regular part and the corresponding products are integrated in turn.

2.2 Form of Thickness Distribution and t'

We will assume that t is expanded about the leading edge in a generalized form of the NACA four- and five-digit airfoil series[26]

$$\frac{t}{c} = A_0\sqrt{\frac{x}{c} + \frac{1}{2}} + \sum_{n=1}^{\infty} A_n\left(\frac{x}{c} + \frac{1}{2}\right)^n \tag{2.3}$$

where A_0 , A_1 , A_2 ... are known constants and finite in number for the NACA four- and five-digit sections and may be found by appropriate curve fitting for others. The leading coefficient A_0 is related to the airfoil leading-edge radius r by

$$A_0 = \sqrt{2r/c} \tag{2.4}$$

This form of the thickness distribution has a square-root behavior at the leading edge only, cf. Refs. 11 and 15 in which the assumed distribution possesses inherently not only a square-root behavior in t at the leading edge but also at the trailing edge as well.

Differentiating Eq. (2.3) and rewriting in a power series in $\bar{x}$ for convenience, we find

$$t' = \frac{a_0}{\sqrt{\lambda+\bar{x}}} + \sum_{n=1}^{\infty} a_n \bar{x}^{n-1} \tag{2.5}$$

where the respective coefficients are related by

$$a_0 = \sqrt{\frac{\lambda}{2}}\, A_0$$

$$a_1 = A_1 + A_2 + \frac{3}{4} A_3 + \frac{1}{2} A_4 + \frac{5}{16} A_5 + \frac{3}{16} A_6 + \frac{7}{64} A_7 + \cdots$$

$$a_2 = \frac{1}{\lambda}\left(A_2 + \frac{3}{2} A_3 + \frac{3}{2} A_4 + \frac{5}{4} A_5 + \frac{15}{16} A_6 + \frac{21}{32} A_7 + \cdots\right)$$

$$a_3 = \frac{1}{\lambda^2}\left(\frac{3}{4} A_3 + \frac{3}{2} A_4 + \frac{15}{8} A_5 + \frac{15}{8} A_6 + \frac{105}{64} A_7 + \cdots\right)$$

$$a_4 = \frac{1}{\lambda^3}\left(\frac{1}{2} A_4 + \frac{5}{4} A_5 + \frac{15}{8} A_6 + \frac{35}{16} A_7 + \cdots\right)$$

$$a_5 = \frac{1}{\lambda^4}\left(\frac{5}{16} A_5 + \frac{15}{16} A_6 + \frac{105}{64} A_7 \cdots\right)$$

$$a_6 = \frac{1}{\lambda^5}\left(\frac{3}{16} A_6 + \frac{21}{32} A_7 + \cdots\right)$$

$$a_7 = \frac{1}{\lambda^6}\left(\frac{7}{64} A_7 + \cdots\right)$$

$$\vdots \qquad (2.6)$$

For NACA four- and five-digit airfoils, these coefficients are tabulated in Table 2.1. From Eq. (2.5) then, we see that t' is composed of a square-root singularity at the leading edge and a regular part.

	$a_n/5\left(\frac{t_{max}}{c}\right)$			
n \ λ	1/4	1/2	3/4	1
0	0.20944	0.29690	0.36363	0.41988
1	-0.63025	-0.63025	-0.63025	-0.63025
2	-0.61920	-0.30960	-0.20640	-0.15480
3	1.95120	0.48780	0.21680	0.12195
4	-6.49600	-0.81200	-0.24059	-0.10150
5	0	0	0	0
.	.	.	.	.
.	.	.	.	.
.	.	.	.	.

TABLE 2.1

COEFFICIENTS OF t'
FOR
NACA FOUR- AND FIVE-DIGIT AIRFOIL SECTIONS

2.3 Form of I_1

Similarly, the second factor in ϵ_t , or

$$I_1 \equiv \frac{1}{2\pi} \{Q'_{\frac{1}{2}}(\tilde{\omega}) - Q'_{-\frac{1}{2}}(\tilde{\omega})\} \tag{2.7}$$

may be separated into two parts, a logarithmic singularity and a regular term $\mathcal{R}_1$. From the known behaviour[22] of $Q_{\frac{1}{2}}$ and $Q_{-\frac{1}{2}}$ near unit argument, we find

$$I_1(\Delta\bar{x}) = -\frac{1}{8\pi} \ell n \frac{\Delta\bar{x}^2}{2} + \mathcal{R}_1(\Delta\bar{x}) \tag{2.8}$$

and both the singular and regular parts are symmetric about $\Delta\bar{x} = 0$. The regular part has been evaluated and is shown in Fig. 2.1.

Since $\mathcal{R}_1(\Delta\bar{x}) = \mathcal{R}_1(\lambda \cos \varphi - \lambda \cos \phi)$ is bounded, it is convenient to expand it in a double Fourier cosine series in the region $0 \leq \phi \leq \pi$ and $0 \leq \varphi \leq \pi$ $(\bar{\xi} = -\lambda \cos \varphi)$ as

$$\mathcal{R}_1 = \sum_{p=0}^{\infty} \sum_{q=0}^{\infty} h_{p,q}(\lambda) \cos p\phi \cos q\varphi \tag{2.9}$$

The coefficients $h_{p,q}(\lambda)$ are, from orthogonality,

$$h_{p,q} = \frac{4}{\pi^2} \int_0^{\pi} \int_0^{\pi} \mathcal{R}_1 \cos p\phi \cos q\varphi \, d\varphi \, d\phi \tag{2.10}$$

for $p,q \neq 0$; $h_{p,0}$ and $h_{0,q}$ are one-half and $h_{0,0}$ is

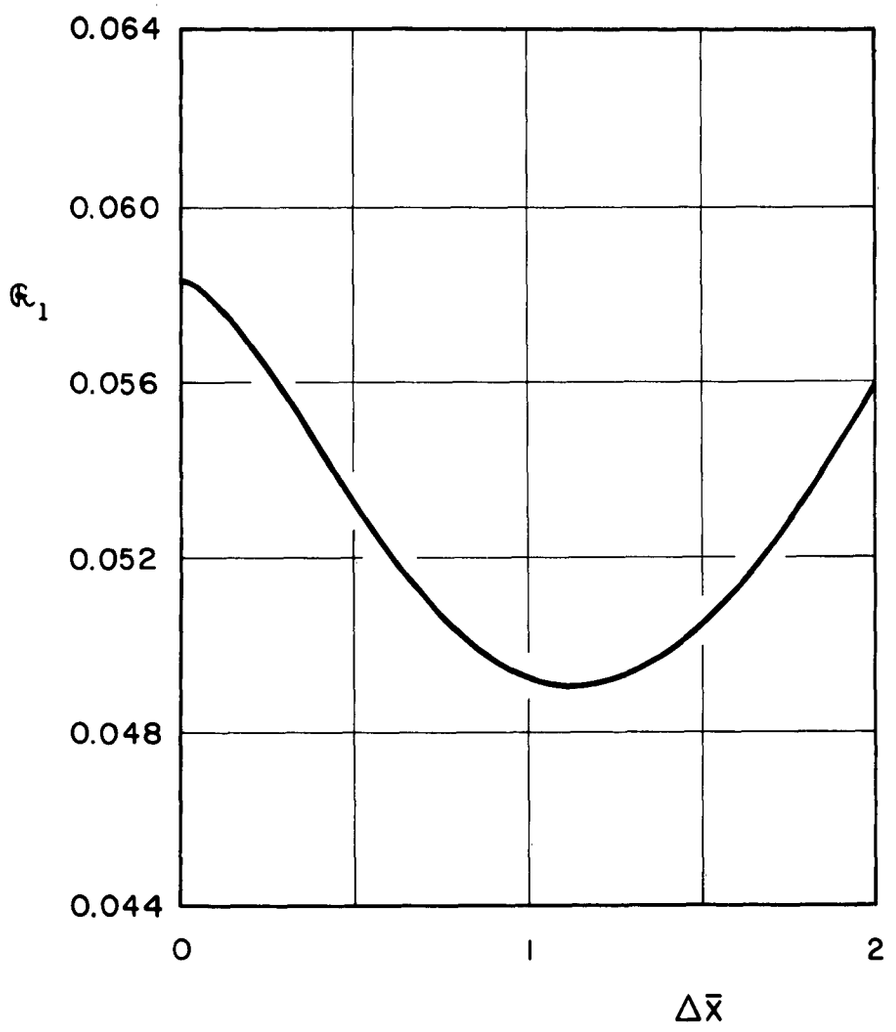

FIGURE 2.1

VARIATION OF REGULAR PART OF I_1

one-quarter of these values. Since $\mathcal{R}_1$ is an even function in $\Delta\bar{x}$, if we interchange ϕ and φ in Eq. (2.10) we can show

$$h_{p,q} = h_{q,p} \tag{2.11}$$

In addition, replacing ϕ by $(\pi-\phi)$ and φ by $(\pi-\varphi)$ in Eq. (2.10), we find

$$h_{p,q} \equiv 0 \quad \text{if} \quad (p+q) = \text{odd integer} \tag{2.12}$$

For $\lambda = 1/4$, $1/2$, $3/4$ and 1 we have computed $h_{p,q}$ for $p,q = 0, 1, 2 \ldots 7$ from Eq. (2.10) using a relaxation procedure developed by G. E. Bartholemew[27]. This was carried out until the difference between successive computations was less than $\pm 1 \times 10^{-5}$ and the results are presented in Tables 2.2-2.5.

A comparison of the exact value of $\mathcal{R}_1$ as obtained from Eqs. (2.7), (2.8) and tables of the Legendre functions[28] with the series value as given by Eq. (2.9) using the computed $h_{p,q}$'s is given in Table 2.6. We find agreement to within $\pm 1 \times 10^{-4}$ in all cases, the results becoming significantly better as λ decreases. This is due to the rapid decay of the $h_{p,q}$ with increasing p and q at low values of λ. As expected, the use of more terms in the double Fourier series gives a higher

p \ q	0	1	2	3	4	5	6	7
0	0.05667	0	-0.00058	0	0.00000	0	0.00000	0
1	0	0.00282	0	-0.00017	0	0.00000	0	0.00000
2	-0.00058	0	0.00033	0	-0.00004	0	0.00000	0
3	0	-0.00017	0	0.00008	0	-0.00002	0	0.00000
4	0.00000	0	-0.00004	0	0.00003	0	-0.00001	0
5	0	0.00000	0	-0.00002	0	0.00001	0	0.00000
6	0.00000	0	0.00000	0	-0.00001	0	0.00001	0
7	0	0.00000	0	0.00000	0	0.00000	0	0.00001

TABLE 2.2

COEFFICIENTS $h_{p,q}$ FOR $\lambda = 1/4$

p \ q	0	1	2	3	4	5	6	7
0	0.05449	0	-0.00090	0	0.00000	0	0.00000	0
1	0	0.00564	0	-0.00067	0	0.00001	0	0.00000
2	-0.00090	0	0.00135	0	-0.00018	0	0.00000	0
3	0	-0.00067	0	0.00034	0	-0.00007	0	0.00000
4	0.00000	0	-0.00018	0	0.00013	0	-0.00003	0
5	0	0.00001	0	-0.00007	0	0.00006	0	-0.00002
6	0.00000	0	0.00000	0	-0.00003	0	0.00004	0
7	0	0.00000	0	0.00000	0	-0.00002	0	0.00002

TABLE 2.3

COEFFICIENTS $h_{p,q}$ **FOR** $\lambda = 1/2$

p \ q	0	1	2	3	4	5	6	7
0	0.05322	0	-0.00042	0	-0.00005	0	0.00000	0
1	0	0.00588	0	-0.00129	0	0.00001	0	0.00000
2	-0.00042	0	0.00274	0	-0.00043	0	0.00001	0
3	0	-0.00129	0	0.00083	0	-0.00016	0	0.00000
4	-0.00005	0	-0.00043	0	0.00031	0	-0.00008	0
5	0	0.00001	0	-0.00016	0	0.00015	0	-0.00004
6	0.00000	0	0.00001	0	-0.00008	0	0.00008	0
7	0	0.00000	0	0.00000	0	-0.00004	0	0.00005

TABLE 2.4

COEFFICIENTS $h_{p,q}$ **FOR** $\lambda = 3/4$

p \ q	0	1	2	3	4	5	6	7
0	0.05309	0	0.00070	0	-0.00016	0	0.00001	0
1	0	0.00356	0	-0.00170	0	-0.00001	0	0.00000
2	0.00070	0	0.00402	0	-0.00075	0	0.00001	0
3	0	-0.00170	0	0.00148	0	-0.00031	0	0.00001
4	-0.00016	0	-0.00075	0	0.00059	0	-0.00015	0
5	0	-0.00001	0	-0.00031	0	0.00028	0	-0.00008
6	0.00001	0	0.00001	0	-0.00015	0	0.00015	0
7	0	0.00000	0	0.00001	0	-0.00008	0	0.00009

TABLE 2.5

COEFFICIENTS $h_{p,q}$ **FOR** $\lambda = 1$

λ	$\bar{x}$	$\bar{\xi}$	$\mathcal{R}_1$		
			Exact	Series p,q=0,1,...6	Series p,q=0,1,...7
1/4	$-\lambda$	$-\lambda$	0.05832	0.05831	0.05831
	$-\lambda$	λ	0.05324	0.05324	0.05324
1/2	$-\lambda$	$-\lambda$	0.05832	0.05834	0.05833
	$-\lambda$	λ	0.04920	0.04921	0.04920
3/4	$-\lambda$	$-\lambda$	0.05832	0.05839	0.05836
	$-\lambda$	λ	0.05046	0.05048	0.05047
1	$-\lambda$	$-\lambda$	0.05832	0.05845	0.05841
	$-\lambda$	λ	0.05591	0.05595	0.05593

TABLE 2.6

COMPARISON OF SERIES APPROXIMATION WITH EXACT VALUE OF $\mathcal{R}_1$

degree of accuracy.

An independent check on the accuracy of the relaxation technique was desired. Accordingly, by the change of variables $y = \bar{x} + \bar{\xi}$, $\eta = \bar{x} - \bar{\xi}$, we found it possible to perform analytically the integration on y and so reduce $h_{p,q}$ to the evaluation of a single integral. Unfortunately, except for $h_{0,0}$, the complexity of the integrand precludes the possibility of further numerical computation; $h_{0,0}$ becomes

$$h_{0,0} = \frac{8}{\pi^2} \int_0^{2\lambda} \frac{\mathcal{R}_1(\eta)}{2\lambda - \eta} Q_{-\frac{1}{2}} \{1 + 16\lambda\eta(2\lambda-\eta)^{-2}\} \, d\eta \qquad (2.13)$$

This was evaluated for $\lambda = 1/2$ and 1 and the results agree to within one unit in the fifth decimal place with those determined by the relaxation method.

With the expansion of both t' and I_1 into a singular and a regular part, we may proceed to the determination of $\{\epsilon_t\}$. The integral form of ϵ_t , Eq. (1.14), can be separated into four components corresponding to the multiplication of the singular-singular, singular-regular, regular-singular, and regular-regular parts of t' and I_1 respectively. We will now consider the evaluation of each of these in turn and the subsequent decomposition of $\{\epsilon_t\}$ into the matrix form $[Q]\{a\}$.

2.4 Singular-Singular Contribution

The first contribution to ϵ_t arises from the product of the two singular terms. Upon integration by parts and transformation to the Glauert angular variable ϕ, we find

$$\int_{-\lambda}^{\lambda} \frac{a_0}{\sqrt{\lambda+\bar{\xi}}} \left(-\frac{1}{8\pi} \ell n \frac{\Delta\bar{x}^2}{2}\right) d\bar{\xi} =$$

$$\frac{1}{\pi}\sqrt{\frac{\lambda}{2}}\left[2 + \tfrac{1}{2}\ell n\frac{2}{\lambda^2} - \ell n(1+\cos\phi) - \sin\tfrac{1}{2}\phi \; \ell n\frac{1+\sin\frac{1}{2}\phi}{1-\sin\frac{1}{2}\phi}\right] a_0 \qquad (2.14)$$

The quantity inside the brackets is finite for $0 \leq \phi \leq \pi$ as can be verified by passing to the appropriate limits.

To obtain the contribution to $\{\epsilon_t\}$, Eq. (2.14) is substituted into Eqs. (1.22) and the necessary integrations carried out using elementary integrals and

$$\int_0^{\pi} \ell n(1+\cos\phi)\, d\phi = -\pi \ell n\, 2 \qquad (2.15)$$

$$\int_0^{\pi} \cos n\phi \; \ell n(1+\cos\phi)\, d\phi = \frac{(-1)^{n+1}\pi}{n} \quad , \quad n \geq 1 \qquad (2.16)$$

$$\int_0^{\pi} \sin\phi \; \ell n\frac{1+\sin\phi}{1-\sin\phi}\, d\phi = 2\pi \qquad (2.17)$$

and

$$\int_0^{\pi} \cos^{2n}\phi \sin\phi \, \ell n\frac{1+\sin\phi}{1-\sin\phi} \, d\phi =$$

$$\frac{2\pi}{2n+1} \frac{1 \cdot 3 \cdot 5 \cdot \cdots (2n-1)}{2 \cdot 4 \cdot 6 \cdot \cdots (2n)} \quad , \quad n \geq 1 \tag{2.18}$$

Eq. (2.15) is taken from Ref. 20. Derivations of Eqs. (2.16), (2.17) and (2.18) may be found in the Appendix.

With these results, the contribution to $\{\epsilon_t\}$ may be written in the matrix form $[Q_{SS}][a]$ where $[Q_{SS}]$ is given in Table 2.7.

2.5 Singular-Regular Contribution

In view of the form of the expansion of $\mathcal{R}_1$ in Eq. (2.9), the contribution to ϵ_t of the product of the singular part of t' and the regular part of I_1 reduces immediately to a Fourier cosine series, or

$$\int_{-\lambda}^{\lambda} \frac{a_0}{\sqrt{\lambda+\bar{\xi}}} \sum_{p=0}^{\infty} \sum_{q=0}^{\infty} h_{p,q} \cos p\phi \cos q\varphi \, d\bar{\xi} =$$

$$\sum_{p=0}^{\infty} \cos p\phi \left[2\sqrt{2\lambda} \sum_{q=0}^{\infty} h_{p,q} \, (-1)^{q+1} / (4q^2-1) \right] a_0 \tag{2.19}$$

To carry this out, we have changed to the Glauert variable and used the relationship $\sin \tfrac{1}{2}\varphi = \sqrt{\tfrac{1}{2}(1-\cos\varphi)}$. Thus the contribution to $\{\epsilon_t\}$ may be written simply by comparison with Eq. (2.1).

$$\frac{2\sqrt{2\lambda}}{\pi}\begin{bmatrix} \frac{1}{4}\ln\frac{8}{\lambda^2} & 0 & 0 & 0 & 0 & 0 & 0 & \cdots \\ -\frac{1}{3} & 0 & 0 & 0 & 0 & 0 & 0 & \\ \frac{1}{30} & 0 & 0 & 0 & 0 & 0 & 0 & \\ -\frac{1}{105} & 0 & 0 & 0 & 0 & 0 & 0 & \\ \frac{1}{252} & 0 & 0 & 0 & 0 & 0 & 0 & \\ -\frac{1}{495} & 0 & 0 & 0 & 0 & 0 & 0 & \\ \frac{1}{858} & 0 & 0 & 0 & 0 & 0 & 0 & \\ \vdots & & & & & & & \end{bmatrix}$$

TABLE 2.7

ELEMENTS OF $[Q_{SS}]$

Similarly to the preceding contribution, this may be expressed as $[Q_{SR}]\{a\}$ with $[Q_{SR}]$ given in Table 2.8.

2.6 Regular-Singular Contribution

The product of the regular part of t' and the singular part of I_1 combine to give

$$\int_{-\lambda}^{\lambda} \sum_{n=1}^{\infty} a_n \bar{\xi}^{n-1} \left(- \frac{1}{8\pi} \ell n \frac{\Delta\bar{x}^2}{2} \right) d\bar{\xi} =$$

$$\sum_{n=1}^{\infty} \frac{1}{8\pi n} \left[-2 \int_{-\lambda}^{\lambda} \frac{\bar{\xi}^n}{\Delta\bar{x}} d\bar{\xi} + \lambda^n \ell n \frac{2}{(\lambda-\bar{x})^2} - (-\lambda)^n \ell n \frac{2}{(\lambda+\bar{x})^2} \right] a_n \qquad (2.20)$$

The integrals on the right-hand side have been evaluated analytically[29], e. g.,

$$\int_{-\lambda}^{\lambda} \frac{\bar{\xi}}{\Delta\bar{x}} d\bar{\xi} = \bar{x} \ell n \frac{\lambda+\bar{x}}{\lambda-\bar{x}} - 2\lambda$$

$$\int_{-\lambda}^{\lambda} \frac{\bar{\xi}^2}{\Delta\bar{x}} d\bar{\xi} = \bar{x}^2 \ell n \frac{\lambda+\bar{x}}{\lambda-\bar{x}} - 2\lambda\bar{x}$$

$$\vdots \qquad (2.21)$$

The reduction of Eq. (2.20) to the matrix form $[Q_{RS}]\{a\}$ is quite lengthy. To illustrate we will consider only a typical case,

$$4\sqrt{2\lambda}\begin{bmatrix}
(h_{0,0} - \frac{1}{15}h_{0,2} - \frac{1}{63}h_{0,4} - \frac{1}{143}h_{0,6} + \ldots) & 0 & 0 & 0 & 0 & 0 & 0 \ldots \\
(-\frac{1}{3}h_{1,1} - \frac{1}{35}h_{1,3} - \frac{1}{99}h_{1,5} - \frac{1}{195}h_{1,7} + \ldots) & 0 & 0 & 0 & 0 & 0 & 0 \\
(-h_{2,0} + \frac{1}{15}h_{2,2} + \frac{1}{63}h_{2,4} + \frac{1}{143}h_{2,6} + \ldots) & 0 & 0 & 0 & 0 & 0 & 0 \\
(-\frac{1}{3}h_{3,1} - \frac{1}{35}h_{3,3} - \frac{1}{99}h_{3,5} - \frac{1}{195}h_{3,7} + \ldots) & 0 & 0 & 0 & 0 & 0 & 0 \\
(-h_{4,0} + \frac{1}{15}h_{4,2} + \frac{1}{63}h_{4,4} + \frac{1}{143}h_{4,6} + \ldots) & 0 & 0 & 0 & 0 & 0 & 0 \\
(-\frac{1}{3}h_{5,1} - \frac{1}{35}h_{5,3} - \frac{1}{99}h_{5,5} - \frac{1}{195}h_{5,7} + \ldots) & 0 & 0 & 0 & 0 & 0 & 0 \\
(-h_{6,0} + \frac{1}{15}h_{6,2} + \frac{1}{63}h_{6,4} + \frac{1}{143}h_{6,6} + \ldots) & 0 & 0 & 0 & 0 & 0 & 0 \\
\vdots & & & & & &
\end{bmatrix}$$

TABLE 2.8

ELEMENTS OF $[Q_{SR}]$

say $n = 1$. From the first of Eqs. (2.21) and Eq. (2.20), this term becomes, after changing to the Glauert variable and rearranging,

$$\frac{\lambda}{4\pi}\left[2 + \ell n\frac{2}{\lambda^2} - (1-\cos\phi)\,\ell n(1-\cos\phi) - (1+\cos\phi)\,\ell n(1+\cos\phi)\right] a_1$$

If we replace $\ell n(1-\cos\phi)$ with $\ell n\, 2\sin^2\tfrac{1}{2}\phi$ and $\ell n(1+\cos\phi)$ with $\ell n\, 2\cos^2\tfrac{1}{2}\phi$ and expand the resulting forms by means of formulas 603.2 and 603.4 of Ref. 20 we get

$$\frac{\lambda}{2\pi}\left[\ell n\frac{8}{\lambda^2} - \frac{1}{3}\cos 2\phi - \frac{1}{30}\cos 4\phi - \frac{1}{105}\cos 6\phi - \ldots\right] a_1$$

Again, the contribution of this term to $\{\epsilon_t\}$ is found by comparison with Eq. (2.1). In a like manner, the contributions of the other terms are obtained and so $[Q_{RS}]$, see Table 2.9.

2.7 Regular-Regular Contribution

The final contribution to $\{\epsilon_t\}$ from the regular parts of t' and I_1 is determined in the same fashion as the singular-regular term. Here, this requires the evaluation of integrals whose integrand is of the form $\bar{\xi}^{n-1}\cos q\varphi$. This is carried out by changing to the Glauert variable and replacing $\cos^{n-1}\varphi$ by its alternate cosine series, cf. formulas 404, Ref. 20. The resulting integrals follow in turn from

$$\frac{2\lambda}{\pi}\begin{bmatrix}
0 & \frac{1}{4}\ell n\frac{8}{\lambda^2} & 0 & \frac{\lambda^2}{12}\ell n\frac{8}{\lambda^2} & 0 & \frac{\lambda^4}{20}\ell n\frac{8}{\lambda^2} & 0 & \cdots \\
0 & 0 & \frac{\lambda}{3} & 0 & \frac{\lambda^3}{5} & 0 & \frac{\lambda^5}{7} & \\
0 & \frac{1}{6} & 0 & \frac{\lambda^2}{30} & 0 & \frac{3\lambda^4}{70} & 0 & \\
0 & 0 & \frac{\lambda}{15} & 0 & \frac{\lambda^3}{105} & 0 & \frac{\lambda^5}{189} & \\
0 & \frac{1}{60} & 0 & \frac{13\lambda^2}{420} & 0 & \frac{17\lambda^4}{1260} & 0 & \\
0 & 0 & \frac{\lambda}{105} & 0 & \frac{\lambda^3}{63} & 0 & \frac{37\lambda^5}{3465} & \\
0 & \frac{1}{210} & 0 & \frac{11\lambda^2}{1890} & 0 & \frac{61\lambda^4}{6930} & 0 & \\
\vdots & & & & & & &
\end{bmatrix}$$

TABLE 2.9

ELEMENTS OF $[Q_{RS}]$

$$\int_0^{\pi} \cos m\varphi \cos q\varphi \sin \varphi \, d\varphi = \frac{[(-1)^{q+m}-1][q^2+(m^2-1)]}{[q^2-(m-1)^2][q^2-(m+1)^2]} \qquad (2.22)$$

which is derived by expressing the integrand as a sum of sine functions, and is valid for $m , q \neq 0$.

In Table 2.10 the corresponding matrix $[Q_{RR}]$ is given.

2.8 Final Form of Effective Camber

With Tables 2.7-2.10 combined to give

$$[Q] \equiv [Q_{SS}] + [Q_{SR}] + [Q_{RS}] + [Q_{RR}] \qquad (2.23)$$

we obtain

$$\{\epsilon_t\} = [Q]\{a\} \qquad (2.24)$$

The leading forty-nine elements of $[Q]$ have been computed to an accuracy of $\pm 1 \times 10^{-4}$ for $\lambda = 1/4 , 1/2 , 3/4$ and 1 and these are presented in Tables 2.11-2.14. Tables 2.2-2.5 were used to compute the elements of $[Q_{SR}]$ and $[Q_{RR}]$.

In summary then, we have from Eq. (2.2)

$$\{c^{2-D}\} = \{\epsilon\} - [Q]\{a\} \qquad (2.25)$$

where the elements of $\{a\}$ are related to the coefficients of

$$
2\lambda \begin{bmatrix}
0 & (h_{0,0} - \frac{1}{3} h_{0,2} - \frac{1}{15} h_{0,4} - \frac{1}{35} h_{0,6} + \ldots) & 0 \\
0 & 0 & (\frac{1}{3} h_{1,1} - \frac{1}{5} h_{1,3} - \frac{1}{21} h_{1,5} - \frac{1}{45} h_{1,7} + \ldots)\lambda \\
0 & (- h_{2,0} + \frac{1}{3} h_{2,2} + \frac{1}{15} h_{2,4} + \frac{1}{35} h_{2,6} + \ldots) & 0 \\
0 & 0 & (\frac{1}{3} h_{3,1} - \frac{1}{5} h_{3,3} - \frac{1}{21} h_{3,5} - \frac{1}{45} h_{3,7} + \ldots)\lambda \\
0 & (- h_{4,0} + \frac{1}{3} h_{4,2} + \frac{1}{15} h_{4,4} + \frac{1}{35} h_{4,6} + \ldots) & 0 \\
0 & 0 & (\frac{1}{3} h_{5,1} - \frac{1}{5} h_{5,3} - \frac{1}{21} h_{5,5} - \frac{1}{45} h_{5,7} + \ldots)\lambda \\
0 & (- h_{6,0} + \frac{1}{3} h_{6,2} + \frac{1}{15} h_{6,4} + \frac{1}{35} h_{6,6} + \ldots) & 0 \\
\vdots & & \\
\end{bmatrix}
$$

	$(\frac{1}{3} h_{0,0} + \frac{1}{15} h_{0,2} - \frac{13}{105} h_{0,4} - \frac{11}{315} h_{0,6} + \ldots) \lambda^2$	0
$\ldots) \lambda$	0	$(\frac{1}{5} h_{1,1} - \frac{1}{35} h_{1,3} - \frac{5}{63} h_{1,5} - \frac{13}{495} h_{1,7} + \ldots) \lambda^3$
	$(-\frac{1}{3} h_{2,0} - \frac{1}{15} h_{2,2} + \frac{13}{105} h_{2,4} + \frac{11}{315} h_{2,6} + \ldots) \lambda^2$	0
$\ldots) \lambda$	0	$(\frac{1}{5} h_{3,1} - \frac{1}{35} h_{3,3} - \frac{5}{63} h_{3,5} - \frac{13}{495} h_{3,7} + \ldots) \lambda^3$
	$(-\frac{1}{3} h_{4,0} - \frac{1}{15} h_{4,2} + \frac{13}{105} h_{4,4} + \frac{11}{315} h_{4,6} + \ldots) \lambda^2$	0
$\ldots) \lambda$	0	$(\frac{1}{5} h_{5,1} - \frac{1}{35} h_{5,3} - \frac{5}{63} h_{5,5} - \frac{13}{495} h_{5,7} + \ldots) \lambda^3$
	$(-\frac{1}{3} h_{6,0} - \frac{1}{15} h_{6,2} + \frac{13}{105} h_{6,4} + \frac{11}{315} h_{6,6} + \ldots) \lambda^2$	0

TABLE 2.10

MATRIX $[Q_{RR}]$

$$(\tfrac{1}{5} h_{0,0} + \tfrac{3}{35} h_{0,2} - \tfrac{17}{315} h_{0,4} - \tfrac{61}{1155} h_{0,6} + \ldots) \lambda^4 \qquad 0$$

$$h_{1,7} + \ldots) \lambda^3 \qquad 0 \qquad (\tfrac{1}{7} h_{1,1} + \tfrac{1}{63} h_{1,3} - \tfrac{37}{693} h_{1,5} - \tfrac{47}{1287} h_{1,7}$$

$$(-\tfrac{1}{5} h_{2,0} - \tfrac{1}{35} h_{2,2} + \tfrac{17}{315} h_{2,4} + \tfrac{61}{1155} h_{2,6} + \ldots) \lambda^4 \qquad 0$$

$$h_{3,7} + \ldots) \lambda^3 \qquad 0 \qquad (\tfrac{1}{7} h_{3,1} + \tfrac{1}{63} h_{3,3} - \tfrac{37}{693} h_{3,5} - \tfrac{47}{1287} h_{3,7}$$

$$(-\tfrac{1}{5} h_{4,0} - \tfrac{1}{35} h_{4,2} + \tfrac{17}{315} h_{4,4} + \tfrac{61}{1155} h_{4,6} + \ldots) \lambda^4 \qquad 0$$

$$h_{5,7} + \ldots) \lambda^3 \qquad 0 \qquad (\tfrac{1}{7} h_{5,1} + \tfrac{1}{63} h_{5,3} - \tfrac{37}{693} h_{5,5} - \tfrac{47}{1287} h_{5,7}$$

$$(-\tfrac{1}{5} h_{6,0} - \tfrac{1}{35} h_{6,2} + \tfrac{17}{315} h_{6,4} + \tfrac{61}{1155} h_{6,6} + \ldots) \lambda^4 \qquad 0$$

$$\begin{pmatrix} (\frac{1}{5} h_{0,0} + \frac{3}{35} h_{0,2} - \frac{17}{315} h_{0,4} - \frac{61}{1155} h_{0,6} + \ldots) \lambda^4 & 0 & \cdots \\ 0 & (\frac{1}{7} h_{1,1} + \frac{1}{63} h_{1,3} - \frac{37}{693} h_{1,5} - \frac{47}{1287} h_{1,7} + \ldots) \lambda^5 & \\ (-\frac{1}{5} h_{2,0} - \frac{1}{35} h_{2,2} + \frac{17}{315} h_{2,4} + \frac{61}{1155} h_{2,6} + \ldots) \lambda^4 & 0 & \\ 0 & (\frac{1}{7} h_{3,1} + \frac{1}{63} h_{3,3} - \frac{37}{693} h_{3,5} - \frac{47}{1287} h_{3,7} + \ldots) \lambda^5 & \\ (-\frac{1}{5} h_{4,0} - \frac{1}{35} h_{4,2} + \frac{17}{315} h_{4,4} + \frac{61}{1155} h_{4,6} + \ldots) \lambda^4 & 0 & \\ 0 & (\frac{1}{7} h_{5,1} + \frac{1}{63} h_{5,3} - \frac{37}{693} h_{5,5} - \frac{47}{1287} h_{5,7} + \ldots) \lambda^5 & \\ (-\frac{1}{5} h_{6,0} - \frac{1}{35} h_{6,2} + \frac{17}{315} h_{6,4} + \frac{61}{1155} h_{6,6} + \ldots) \lambda^4 & 0 & \end{pmatrix}$$

0.7064	0.2499	0	0.0052	0	0.0002	0
-0.1527	0	0.0135	0	0.0005	0	0.0000
0.0167	0.0272	0	-0.0003	0	0.0000	0
-0.0041	0	-0.0027	0	0.0000	0	0.0000
0.0018	0.0026	0	0.0003	0	0.0000	0
-0.0009	0	-0.0004	0	0.0000	0	0.0000
0.0005	0.0008	0	0.0001	0	0.0000	0

TABLE 2.11

ELEMENTS OF [Q] FOR $\lambda = 1/4$

$$
\begin{bmatrix}
0.7698 & 0.3854 & 0 & 0.0320 & 0 & 0.0048 & 0 \\
-0.2197 & 0 & 0.0551 & 0 & 0.0082 & 0 & 0.0015 \\
0.0252 & 0.0557 & 0 & -0.0026 & 0 & -0.0009 & 0 \\
-0.0052 & 0 & -0.0109 & 0 & -0.0004 & 0 & 0.0001 \\
0.0025 & 0.0052 & 0 & 0.0025 & 0 & 0.0003 & 0 \\
-0.0013 & 0 & -0.0015 & 0 & -0.0006 & 0 & -0.0001 \\
0.0007 & 0.0015 & 0 & 0.0005 & 0 & 0.0002 & 0
\end{bmatrix}
$$

TABLE 2.12

ELEMENTS OF [Q] FOR $\lambda = 1/2$

0.7784	0.4770	0	0.0893	0	0.0301	0
-0.2693	0	0.1244	0	0.0418	0	0.0168
0.0289	0.0835	0	-0.0091	0	-0.0066	0
-0.0054	0	-0.0252	0	-0.0023	0	0.0005
0.0032	0.0077	0	0.0085	0	0.0021	0
-0.0016	0	-0.0033	0	-0.0032	0	-0.0012
0.0008	0.0022	0	0.0015	0	0.0013	0

TABLE 2.13

ELEMENTS OF [Q] **FOR** $\lambda = 3/4$

$$
\begin{bmatrix}
0.7681 & 0.5424 & 0 & 0.1814 & 0 & 0.1089 & 0 \\
-0.3066 & 0 & 0.2183 & 0 & 0.1304 & 0 & 0.0929 \\
0.0275 & 0.1085 & 0 & -0.0236 & 0 & -0.0294 & 0 \\
-0.0056 & 0 & -0.0458 & 0 & -0.0075 & 0 & 0.0026 \\
0.0043 & 0.0104 & 0 & 0.0204 & 0 & 0.0091 & 0 \\
-0.0018 & 0 & -0.0059 & 0 & -0.0102 & 0 & -0.0069 \\
0.0010 & 0.0030 & 0 & 0.0036 & 0 & 0.0056 & 0
\end{bmatrix}
$$

TABLE 2.14

ELEMENTS OF [Q] **FOR** $\lambda = 1$

the thickness distribution by Eqs. (2.6). Consequently, the contribution of shroud thickness has been simplified to a single matrix operation on these related coefficients.

CHAPTER THREE

DUCT PRESSURE DISTRIBUTION, SECTIONAL RADIAL FORCE AND PITCHING MOMENT

3.1 Linearized Value of c_p

The duct surface pressure coefficient c_p is defined by

$$c_p \equiv \frac{p-p_\infty}{\frac{1}{2}\rho U^2} \tag{3.1}$$

where p is the local static pressure, p_∞ the free stream static pressure and ρ the fluid density. Consistent with our assumption of small perturbations, we use the linearized form of Bernoulli's equation, or

$$p - p_\infty = - \rho U \{u_f(\bar{x},1) + u_\gamma(\bar{x},1)\} \tag{3.2}$$

With this result and Eqs. (1.8), (1.10), (1.13) and (1.17), Eq. (3.1) reduces to

$$c_p = \pm\, c(\bar{x}) + \frac{1}{\pi} \int_{-\lambda}^{\lambda} t'(\bar{\xi})\, \Delta\bar{x}\, Q'_{-\frac{1}{2}}(\tilde{\omega})\, d\bar{\xi}$$

$$- \frac{1}{\pi} \int_{-\lambda}^{\lambda} c(\bar{\xi}) \{Q'_{\frac{1}{2}}(\tilde{\omega}) - Q'_{-\frac{1}{2}}(\tilde{\omega})\}\, d\bar{\xi} \tag{3.3}$$

and the net duct loading, or the inner surface pressure coefficient

minus the outer surface pressure coefficient, is simply

$$c_p] = -2\,C(\bar{x}) \tag{3.4}$$

We see that c_p is composed of a discontinuous part proportional to the local vortex strength and a continuous part composed of a term due directly to the duct thickness and a term due to the vortex distribution, or equivalently, the effective camber. Analogously to the thickness-induced camber, the contributions to the continuous part may be reduced to a matrix operation on the duct sectional properties. This is readily seen for the second integral if we compare the integrands of $v_f(\bar{x},1)$ and $u_\gamma(\bar{x},1)$, Eqs. (1.9) and (1.10), and note the form of $C(\bar{x})$, Eq. (1.19). For the first integral, however, it is necessary to put the second factor in the integrand, say I_2, in a suitable form.

3.2 Form of I_2

We now consider I_2, or

$$I_2 \equiv \frac{1}{2\pi}\,\Delta\bar{x}\; Q'_{-\frac{1}{2}}(\tilde{\omega}) \tag{3.5}$$

Physically, I_2 is equal to the axial velocity induced on the reference cylinder by a ring source of unit strength having the

same radius. From the known logarithmic behaviour of $Q_{-\frac{1}{2}}$ near unit argument, we find that I_2 may be separated into two parts; a Cauchy singular term and a regular term $\mathcal{R}_2$, or

$$I_2(\Delta\bar{x}) = -\frac{1}{2\pi\Delta\bar{x}} + \mathcal{R}_2(\Delta\bar{x}) \tag{3.6}$$

Both the regular and singular parts are antisymmetric about $\Delta\bar{x} = 0$. The regular part has been computed and is shown in Fig. 3.1. It has been checked against the corresponding function U_{xq} ($U_{xq} = -2\pi\,\mathcal{R}_2$) previously tabulated by Weissinger[15].

As in the case of $\mathcal{R}_1$, we expand $\mathcal{R}_2$ in a double Fourier cosine series in the region $0 \leq \phi \leq \pi$ and $0 \leq \varphi \leq \pi$ as

$$\mathcal{R}_2 = \sum_{p=0}^{\infty}\sum_{q=0}^{\infty} j_{p,q}(\lambda)\cos p\phi \cos q\varphi \tag{3.7}$$

where the coefficients $j_{p,q}$ are given by Eq. (2.10) with $\mathcal{R}_1$ replaced by $\mathcal{R}_2$ and $h_{p,q}$ by $j_{p,q}$. Since $\mathcal{R}_2$ is an odd function in $\Delta\bar{x}$, we can show by interchanging ϕ and φ that

$$j_{p,q} = -j_{q,p} \tag{3.8}$$

As a result, $j_{0,0}$, $j_{1,1}$, $j_{2,2}$, ... all identically vanish. Also, by replacing ϕ by $(\pi-\phi)$ and φ by $(\pi-\varphi)$, we find

$$j_{p,q} = 0 \qquad \text{if } (p+q) = \text{even integer} \tag{3.9}$$

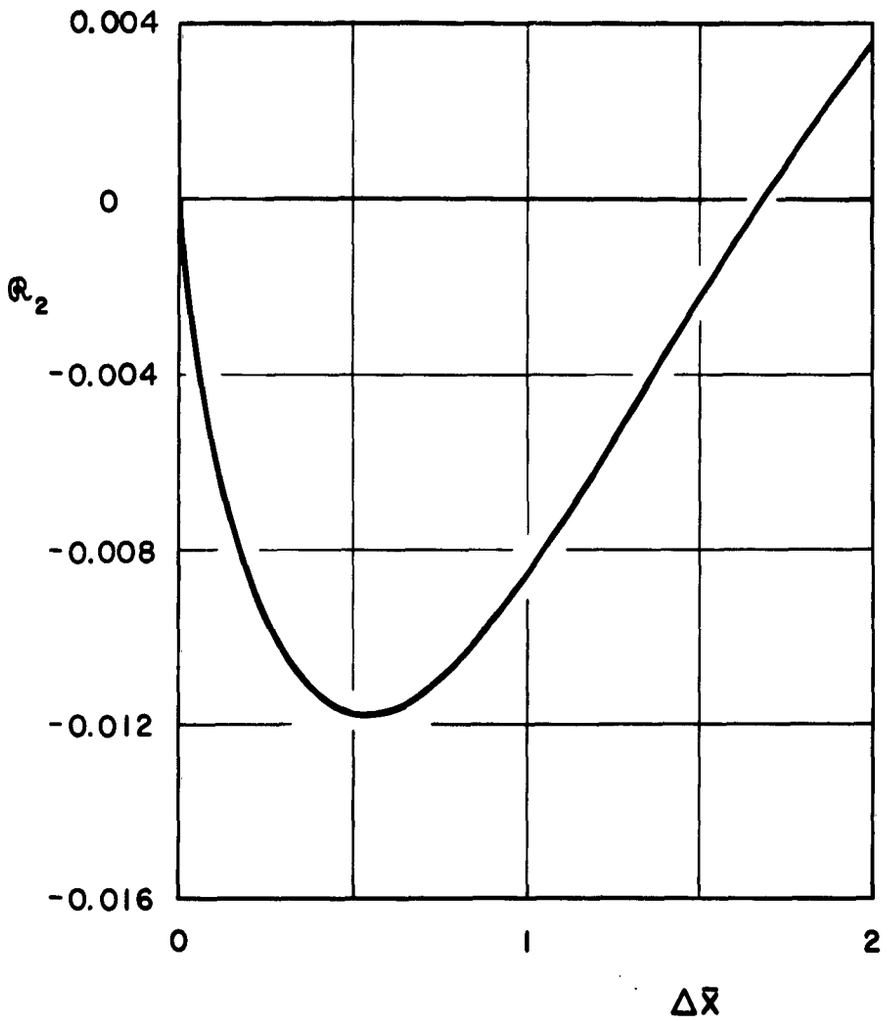

FIGURE 3.1

VARIATION OF REGULAR PART OF I_2

Using the relaxation procedure mentioned earlier, we have computed $j_{p,q}$ for $p,q = 0, 1, 2, \ldots 7$ for $\lambda = 1/4$, $1/2$, $3/4$ and 1 until the difference between successive computations was less than $\pm 1 \times 10^{-5}$ and the results are presented in Tables 3.1-3.4. Table 3.5 gives a comparison between the exact value of $\mathcal{R}_2$ and the series value obtained using the computed $j_{p,q}$. Agreement is to within $\pm 5 \times 10^{-4}$, with the series value for the smaller λ's again being significantly better.

With the expansion of I_2 into a singular and a regular part, the direct-thickness contribution to c_p can be simplified to matrix form.

3.3 Reduction of Direct-Thickness Contribution

Since each of the two factors in the integrand of the direct-thickness contribution is composed of a singular and a regular part, the contribution of this term to c_p could be reduced to matrix form in exactly the same fashion as was the thickness-induced camber. That is, we would consider the product of the singular-singular, singular-regular, regular-singular and regular-regular parts and evaluate each in turn. However, it is more convenient to break up the integration in the following manner.

First consider the product of t' and the Cauchy singular part of I_2, or

p \ q	0	1	2	3	4	5	6	7
0	0	0.00795	0	-0.00001	0	0.00001	0	0.00001
1	-0.00795	0	0.00264	0	0.00001	0	0.00002	0
2	0	-0.00264	0	0.00085	0	0.00001	0	0.00002
3	0.00001	0	-0.00085	0	0.00042	0	0.00002	0
4	0	-0.00001	0	-0.00042	0	0.00026	0	0.00000
5	-0.00001	0	-0.00001	0	-0.00026	0	0.00017	0
6	0	-0.00002	0	-0.00002	0	-0.00017	0	0.00013
7	-0.00001	0	-0.00002	0	0.00000	0	-0.00013	0

TABLE 3.1

COEFFICIENTS $j_{p,q}$ FOR $\lambda = 1/4$

p \ q	0	1	2	3	4	5	6	7
0	0	0.00842	0	-0.00001	0	0.00002	0	0.00000
1	-0.00842	0	0.00539	0	-0.00004	0	0.00001	0
2	0	-0.00539	0	0.00180	0	-0.00001	0	0.00001
3	0.00001	0	-0.00180	0	0.00086	0	0.00000	0
4	0	0.00004	0	-0.00086	0	0.00051	0	0.00000
5	0.00000	0	0.00001	0	-0.00051	0	0.00034	0
6	0	-0.00001	0	0.00000	0	-0.00034	0	0.00024
7	0.00000	0	-0.00001	0	0.00000	0	-0.00024	0

TABLE 3.2

COEFFICIENTS $j_{p,q}$ **FOR** $\lambda = 1/2$

p \ q	0	1	2	3	4	5	6	7
0	0	0.00649	0	0.00015	0	-0.00001	0	0.00000
1	-0.00649	0	0.00756	0	-0.00009	0	0.00000	0
2	0	-0.00756	0	0.00286	0	-0.00004	0	0.00000
3	-0.00015	0	-0.00286	0	0.00136	0	-0.00001	0
4	0	0.00009	0	-0.00136	0	0.00078	0	0.00000
5	0.00001	0	0.00004	0	-0.00078	0	0.00051	0
6	0	0.00000	0	0.00001	0	-0.00051	0	0.00036
7	0.00000	0	0.00000	0	0.00000	0	-0.00036	0

TABLE 3.3

COEFFICIENTS $j_{p,q}$ **FOR** $\lambda = 3/4$

p \ q	0	1	2	3	4	5	6	7
0	0	0.00384	0	0.00047	0	-0.00003	0	0.00000
1	-0.00384	0	0.00878	0	-0.00008	0	-0.00001	0
2	0	-0.00878	0	0.00390	0	-0.00007	0	0.00000
3	-0.00047	0	-0.00390	0	0.00191	0	-0.00003	0
4	0	0.00008	0	-0.00191	0	0.00109	0	-0.00001
5	0.00003	0	0.00007	0	-0.00109	0	0.00070	0
6	0	0.00001	0	0.00003	0	-0.00070	0	0.00049
7	0.00000	0	0.00000	0	0.00001	0	-0.00049	0

TABLE 3.4

COEFFICIENTS $j_{p,q}$ **FOR** $\lambda = 1$

λ	$\bar{x}$	ξ	$\mathcal{R}_2$		
			Exact	Series p,q=0,1,...6	Series p,q=0,1,...7
1/4	$-\lambda$	0	0.00960	0.00976	0.00962
	$-\lambda$	λ	0.01177	0.01157	0.01187
1/2	$-\lambda$	0	0.01177	0.01205	0.01181
	$-\lambda$	λ	0.00861	0.00831	0.00883
3/4	$-\lambda$	0	0.01099	0.01139	0.01103
	$-\lambda$	λ	0.00224	0.00182	0.00254
1	$-\lambda$	0	0.00861	0.00916	0.00866
	$-\lambda$	λ	-0.00358	-0.00413	-0.00316

TABLE 3.5

COMPARISON OF SERIES APPROXIMATION WITH EXACT VALUE OF $\mathcal{R}_2$

$$F(\bar{x}) \equiv -\frac{1}{\pi}\int_{-\lambda}^{\lambda}\frac{t'(\bar{\xi})}{\Delta\bar{x}}\,d\bar{\xi} \tag{3.10}$$

This is identified as the thin-airfoil theory formula for the linearized pressure coefficient of a two-dimensional airfoil section with thickness t and no camber, see for example Ref. 30. For NACA sections, values of the local surface velocities have been tabulated in Appendix I of Ref. 36 and it is better to use these more exact values multiplied by (-2) rather than to evaluate the integral of Eq. (3.10).

Since $\mathcal{R}_2$ has been expanded in the same form as $\mathcal{R}_1$, the remainder of the integral, or the product of t' and $\mathcal{R}_2$, follows as in Sections 2.5 and 2.7 using $j_{p,q}$ instead of $h_{p,q}$, or

$$2\int_{-\lambda}^{\lambda} t'(\bar{\xi})\ \mathcal{R}_2(\Delta\bar{x})\,d\bar{\xi} = -\{\phi\}^T[T]\{a\} \tag{3.11}$$

where the minus sign is for convenience later and

$$\{\phi\} \equiv \frac{1}{2}\begin{Bmatrix} 1 \\ -\cos\phi \\ -\cos 2\phi \\ \vdots \end{Bmatrix} \tag{3.12}$$

T denotes the transposed matrix, and $[T]$ is a square matrix whose elements are functions only of λ and are given in Table 3.6.

$$2\lambda \begin{bmatrix} (\frac{1}{3} j_{0,1} + \frac{1}{35} j_{0,3} + \frac{1}{99} j_{0,5} + \frac{1}{195} j_{0,7} + \cdots)\sqrt{\frac{2}{\lambda}} & 0 & (-\frac{1}{3} j_{0,1} + \frac{1}{5} j_{0,} \\ (-j_{1,0} + \frac{1}{15} j_{1,2} + \frac{1}{63} j_{1,4} + \frac{1}{143} j_{1,6} + \cdots)\sqrt{\frac{2}{\lambda}} & (-j_{1,0} + \frac{1}{3} j_{1,2} + \frac{1}{15} j_{1,4} + \frac{1}{35} j_{1,6} + \cdots) & \\ (-\frac{1}{3} j_{2,1} - \frac{1}{35} j_{2,3} - \frac{1}{99} j_{2,5} - \frac{1}{195} j_{2,7} + \cdots)\sqrt{\frac{2}{\lambda}} & 0 & (\frac{1}{3} j_{2,1} - \frac{1}{5} j_{2,} \\ (-j_{3,0} + \frac{1}{15} j_{3,2} + \frac{1}{63} j_{3,4} + \frac{1}{143} j_{3,6} + \cdots)\sqrt{\frac{2}{\lambda}} & (-j_{3,0} + \frac{1}{3} j_{3,2} + \frac{1}{15} j_{3,4} + \frac{1}{35} j_{3,6} + \cdots) & \\ (-\frac{1}{3} j_{4,1} - \frac{1}{35} j_{4,3} - \frac{1}{99} j_{4,5} - \frac{1}{195} j_{4,7} + \cdots)\sqrt{\frac{2}{\lambda}} & 0 & (\frac{1}{3} j_{4,1} - \frac{1}{5} j_{4,} \\ (-j_{5,0} + \frac{1}{15} j_{5,2} + \frac{1}{63} j_{5,4} + \frac{1}{143} j_{5,6} + \cdots)\sqrt{\frac{2}{\lambda}} & (-j_{5,0} + \frac{1}{3} j_{5,2} + \frac{1}{15} j_{5,4} + \frac{1}{35} j_{5,6} + \cdots) & \\ (-\frac{1}{3} j_{6,1} - \frac{1}{35} j_{6,3} - \frac{1}{99} j_{6,5} - \frac{1}{195} j_{6,7} + \cdots)\sqrt{\frac{2}{\lambda}} & 0 & (\frac{1}{3} j_{6,1} - \frac{1}{5} j_{6,} \\ \vdots & & \end{bmatrix}$$

$\frac{1}{3} j_{0,1} + \frac{1}{5} j_{0,3} + \frac{1}{21} j_{0,5} + \frac{1}{45} j_{0,7} + \ldots)\lambda$	0	$(-\frac{1}{5} j_{0,1} + \frac{1}{35} j_{0,3} + \frac{5}{63} j_{0,5} +$
0	$(-\frac{1}{3} j_{1,0} - \frac{1}{15} j_{1,2} + \frac{13}{105} j_{1,4} + \frac{11}{315} j_{1,6} + \ldots)\lambda^2$	0
$(\frac{1}{3} j_{2,1} - \frac{1}{5} j_{2,3} - \frac{1}{21} j_{2,5} - \frac{1}{45} j_{2,7} + \ldots)\lambda$	0	$(\frac{1}{5} j_{2,1} - \frac{1}{35} j_{2,3} - \frac{5}{63} j_{2,5}$
0	$(-\frac{1}{3} j_{3,0} - \frac{1}{15} j_{3,2} + \frac{13}{105} j_{3,4} + \frac{11}{315} j_{3,6} + \ldots)\lambda^2$	0
$(\frac{1}{3} j_{4,1} - \frac{1}{5} j_{4,3} - \frac{1}{21} j_{4,5} - \frac{1}{45} j_{4,7} + \ldots)\lambda$	0	$(\frac{1}{5} j_{4,1} - \frac{1}{35} j_{4,3} - \frac{5}{63} j_{4,5}$
0	$(-\frac{1}{3} j_{5,0} - \frac{1}{15} j_{5,2} + \frac{13}{105} j_{5,4} + \frac{11}{315} j_{5,6} + \ldots)\lambda^2$	0
$(\frac{1}{3} j_{6,1} - \frac{1}{5} j_{6,3} - \frac{1}{21} j_{6,5} - \frac{1}{45} j_{6,7} + \ldots)\lambda$	0	$(\frac{1}{5} j_{6,1} - \frac{1}{35} j_{6,3} - \frac{5}{63} j_{6,5}$

TABLE 3.6

MATRIX [T]

$$j_{0,3} + \frac{5}{63} j_{0,5} + \frac{13}{495} j_{0,7} + \ldots)\lambda^3 \qquad 0 \qquad (-\frac{1}{7} j_{0,1} - \frac{1}{63} j_{0,3} + \frac{37}{693} j_{0,5} + \frac{47}{1287}$$

$$0 \qquad (-\frac{1}{5} j_{1,0} - \frac{3}{35} j_{1,2} + \frac{17}{315} j_{1,4} + \frac{61}{1155} j_{1,6} + \ldots)\lambda^4 \qquad 0$$

$$j_{2,3} - \frac{5}{63} j_{2,5} - \frac{13}{495} j_{2,7} + \ldots)\lambda^3 \qquad 0 \qquad (\frac{1}{7} j_{2,1} + \frac{1}{63} j_{2,3} - \frac{37}{693} j_{2,5} - \frac{47}{1287}$$

$$0 \qquad (-\frac{1}{5} j_{3,0} - \frac{3}{35} j_{3,2} + \frac{17}{315} j_{3,4} + \frac{61}{1155} j_{3,6} + \ldots)\lambda^4 \qquad 0$$

$$j_{4,3} - \frac{5}{63} j_{4,5} - \frac{13}{495} j_{4,7} + \ldots)\lambda^3 \qquad 0 \qquad (\frac{1}{7} j_{4,1} + \frac{1}{63} j_{4,3} - \frac{37}{693} j_{4,5} - \frac{47}{1287}$$

$$0 \qquad (-\frac{1}{5} j_{5,0} - \frac{3}{35} j_{5,2} + \frac{17}{315} j_{5,4} + \frac{61}{1155} j_{5,6} + \ldots)\lambda^4 \qquad 0$$

$$j_{6,3} - \frac{5}{63} j_{6,5} - \frac{13}{495} j_{6,7} + \ldots)\lambda^3 \qquad 0 \qquad (\frac{1}{7} j_{6,1} + \frac{1}{63} j_{6,3} - \frac{37}{693} j_{6,5} - \frac{47}{1287}$$

$$
\begin{bmatrix}
\ldots)\lambda^3 & 0 & (-\frac{1}{7} j_{0,1} - \frac{1}{63} j_{0,3} + \frac{37}{693} j_{0,5} + \frac{47}{1287} j_{0,7} + \ldots)\lambda^5 & \cdots \\
(-\frac{1}{5} j_{1,0} - \frac{3}{35} j_{1,2} + \frac{17}{315} j_{1,4} + \frac{61}{1155} j_{1,6} + \ldots)\lambda^4 & 0 & & \\
\ldots)\lambda^3 & 0 & (\frac{1}{7} j_{2,1} + \frac{1}{63} j_{2,3} - \frac{37}{693} j_{2,5} - \frac{47}{1287} j_{2,7} + \ldots)\lambda^5 & \\
(-\frac{1}{5} j_{3,0} - \frac{3}{35} j_{3,2} + \frac{17}{315} j_{3,4} + \frac{61}{1155} j_{3,6} + \ldots)\lambda^4 & 0 & & \\
\ldots)\lambda^3 & 0 & (\frac{1}{7} j_{4,1} + \frac{1}{63} j_{4,3} - \frac{37}{693} j_{4,5} - \frac{47}{1287} j_{4,7} + \ldots)\lambda^5 & \\
(-\frac{1}{5} j_{5,0} - \frac{3}{35} j_{5,2} + \frac{17}{315} j_{5,4} + \frac{61}{1155} j_{5,6} + \ldots)\lambda^4 & 0 & & \\
\ldots)\lambda^3 & 0 & (\frac{1}{7} j_{6,1} + \frac{1}{63} j_{6,3} - \frac{37}{693} j_{6,5} - \frac{47}{1287} j_{6,7} + \ldots)\lambda^5 &
\end{bmatrix}
$$

The leading forty-nine elements of $[T]$ are given in Tables 3.7-3.10 to an accuracy of $\pm 1 \times 10^{-4}$ for $\lambda = 1/4$, $1/2$, $3/4$ and 1 .

3.4 Reduction of Effective-Camber Contribution

As noted in Section 3.1, the integrand of the effective-camber contribution is already in a form suitable for integration. The reduction is carried out by decomposing the integrand into four parts corresponding to the singular-singular, singular-regular, regular-singular and regular-regular contributions of C and I_1 . Each of these is evaluated in turn as in Sections 2.4-2.7 with the aid of the relationships $\sin n\varphi \cdot \sin \varphi = \frac{1}{2}\{\cos(n-1)\varphi - \cos(n+1)\varphi\}$ and $\cot \frac{1}{2}\varphi = (1+\cos \varphi)/\sin \varphi$ and the following definite integrals which are derived in the Appendix,

$$\int_0^\pi \ell n(\cos\varphi - \cos\phi)^2 \, d\varphi = -\pi \ell n \, 4 \qquad (3.13)$$

$$\int_0^\pi \cos n\varphi \, \ell n(\cos\varphi - \cos\phi)^2 \, d\varphi = -\frac{2\pi}{n} \cos n\phi \, , \; n \geq 1 \qquad (3.14)$$

and

$$\int_0^\pi \sin \nu\varphi \cos q\varphi \sin \varphi \, d\varphi = \frac{\pi}{2} \, , \; \nu = 1 \;\; \& \;\; q = 0$$

$$= \pm \frac{\pi}{4} \, , \; \nu = q \mp 1 \;\; \& \;\; q \geq 1 \qquad (3.15)$$

0.0150	0	-0.0013	0	0.0000	0	0.0000
0.0460	0.0177	0	0.0003	0	0.0000	0
0.0048	0	-0.0004	0	0.0000	0	0.0000
-0.0003	-0.0005	0	0.0000	0	0.0000	0
0.0001	0	0.0000	0	0.0000	0	0.0000
0.0000	0.0000	0	0.0000	0	0.0000	0
0.0001	0	0.0000	0	0.0000	0	0.0000

TABLE 3.7

ELEMENTS OF [T] FOR $\lambda = 1/4$

0.0224	0	-0.0056	0	-0.0008	0	-0.0002
0.0702	0.0408	0	0.0024	0	0.0003	0
0.0140	0	-0.0036	0	-0.0006	0	-0.0001
-0.0009	-0.0022	0	0.0002	0	0.0000	0
0.0000	0	0.0000	0	0.0000	0	0.0000
0.0000	-0.0001	0	-0.0001	0	0.0000	0
0.0000	0	0.0000	0	0.0000	0	0.0000

TABLE 3.8

ELEMENTS OF [T] **FOR** $\lambda = 1/2$

0.0212	0	-0.0096	0	-0.0033	0	-0.0013
0.0685	0.0540	0	0.0056	0	0.0012	0
0.0239	0	-0.0115	0	-0.0040	0	-0.0015
-0.0002	-0.0043	0	0.0014	0	0.0007	0
0.0000	0	-0.0002	0	0.0000	0	-0.0001
-0.0002	-0.0002	0	-0.0003	0	0.0000	0
0.0000	0	-0.0001	0	0.0001	0	0.0000

TABLE 3.9

ELEMENTS OF [T] **FOR** = 3/4

$$
\begin{bmatrix}
0.0146 & 0 & -0.0095 & 0 & -0.0060 & 0 & -0.0045 \\
0.0500 & 0.0541 & 0 & 0.0055 & 0 & 0.0001 & 0 \\
0.0319 & 0 & -0.0241 & 0 & -0.0149 & 0 & -0.0095 \\
0.0028 & -0.0056 & 0 & 0.0052 & 0 & 0.0042 & 0 \\
0.0002 & 0 & -0.0009 & 0 & -0.0001 & 0 & -0.0006 \\
-0.0004 & -0.0005 & 0 & -0.0010 & 0 & -0.0003 & 0 \\
0.0000 & 0 & -0.0006 & 0 & 0.0003 & 0 & 0.0002
\end{bmatrix}
$$

TABLE 3.10

ELEMENTS OF [T] **FOR** $\lambda = 1$

Finally, the four contributions are added together to give the matrix form of the effective-camber contribution, or

$$\frac{1}{\pi}\int_0^{\pi} C(\bar{\xi})\{Q'_{\frac{1}{2}}(\tilde{\omega}) - Q'_{-\frac{1}{2}}(\tilde{\omega})\}\, d\bar{\xi} = \{\phi\}^T[S]\{c\} \qquad (3.16)$$

where $[S]$ is given in Table 3.11. The leading forty-nine elements of $[S]$ have been computed to an accuracy of $\pm 1 \times 10^{-4}$ and are given in Tables 3.12-3.15 for $\lambda = 1/4$, $1/2$, $3/4$ and 1 .

3.5 Final Form of c_p

The final form of the duct surface pressure coefficient is now obtained by substituting Eqs. (3.5), (3.6), (3.10), (3.11), and (3.16) into Eq. (3.3) to get

$$c_p = \pm C(\bar{x}) + F(\bar{x}) - \{\phi\}^T([T]\{a\} + [S]\{c\}) \qquad (3.17)$$

Thus we have succeeded in reducing the calculation of the aerodynamic loading on an annular airfoil to a simple matrix operation on $\{a\}$ and $\{c\}$ or equivalently, on the duct sectional properties A_0 , A_1 , A_2 ... and ϵ_0 , ϵ_1 , ϵ_2 ... since they are related to $\{a\}$ and $\{c\}$ through Eqs. (2.6), (1.20) and (2.25). The matrix method of computing c_p is ideally suited for engineering calculations and preliminary design studies since it is both simple and rapid and the effects of varying any or all

$$
\pi\lambda \begin{bmatrix}
(4\, h_{0,0} + \frac{1}{2\pi} \ln \frac{8}{\lambda^2}) & (2\, h_{0,0} - h_{0,2} + \frac{1}{4\pi} \ln \frac{8}{\lambda^2}) & 0 & (h_{0,2} - h_{0,4}) & 0 \\
(-2\, h_{1,1} - \frac{1}{\pi}) & 0 & (-h_{1,1} + h_{1,3} - \frac{1}{2\pi}) & 0 & (-h_{1,3} + \\
-4\, h_{2,0} & (-2\, h_{2,0} + h_{2,2} + \frac{1}{4\pi}) & 0 & (-h_{2,2} + h_{2,4} - \frac{1}{4\pi}) & 0 \\
-2\, h_{3,1} & 0 & (-h_{3,1} + h_{3,3} + \frac{1}{6\pi}) & 0 & (-h_{3,3} + h_{3,5} \\
-4\, h_{4,0} & (-2\, h_{4,0} + h_{4,2}) & 0 & (-h_{4,2} + h_{4,4} + \frac{1}{8\pi}) & 0 \\
-2\, h_{5,1} & 0 & (-h_{5,1} + h_{5,3}) & 0 & (-h_{5,3} + h_{5,5} \\
-4\, h_{6,0} & (-2\, h_{6,0} + h_{6,2}) & 0 & (-h_{6,2} + h_{6,4}) & 0 \\
\vdots & & & &
\end{bmatrix}
$$

TABLE 3.11

MATRIX [S]

$$
\begin{bmatrix}
0 & (h_{0,2} - h_{0,4}) & 0 & (h_{0,4} - h_{0,6}) & 0 & \cdots \\
(-h_{1,1} + h_{1,3} - \frac{1}{2\pi}) & 0 & (-h_{1,3} + h_{1,5}) & 0 & (-h_{1,5} + h_{1,7}) & \\
0 & (-h_{2,2} + h_{2,4} - \frac{1}{4\pi}) & 0 & (-h_{2,4} + h_{2,6}) & 0 & \\
(-h_{3,1} + h_{3,3} + \frac{1}{6\pi}) & 0 & (-h_{3,3} + h_{3,5} - \frac{1}{6\pi}) & 0 & (-h_{3,5} + h_{3,7}) & \\
0 & (-h_{4,2} + h_{4,4} + \frac{1}{8\pi}) & 0 & (-h_{4,4} + h_{4,6} - \frac{1}{8\pi}) & 0 & \\
(-h_{5,1} + h_{5,3}) & 0 & (-h_{5,3} + h_{5,5} + \frac{1}{10\pi}) & 0 & (-h_{5,5} + h_{5,7} - \frac{1}{10\pi}) & \\
0 & (-h_{6,2} + h_{6,4}) & 0 & (-h_{6,4} + h_{6,6} + \frac{1}{12\pi}) & 0 &
\end{bmatrix}
$$

TABLE 3.11

MATRIX [S]

0.7845	0.3927	0	-0.0005	0	0.0000	0
-0.2544	0	-0.1273	0	0.0001	0	0.0000
0.0018	0.0637	0	-0.0628	0	0.0000	0
0.0003	0	0.0419	0	-0.0417	0	0.0000
0.0000	0.0000	0	0.0313	0	-0.0313	0
0.0000	0	0.0000	0	0.0250	0	-0.0250
0.0000	0.0000	0	0.0000	0	0.0208	0

TABLE 3.12

ELEMENTS OF [S] **FOR** $\lambda = 1/4$

1.2088	0.6058	0	-0.0014	0	0.0000	0
-0.5177	0	-0.2599	0	0.0011	0	0.0000
0.0057	0.1300	0	-0.1274	0	0.0003	0
0.0021	0	0.0849	0	-0.0840	0	0.0001
0.0000	-0.0003	0	0.0630	0	-0.0628	0
0.0000	0	-0.0001	0	0.0502	0	-0.0501
0.0000	0.0000	0	-0.0001	0	0.0418	0

TABLE 3.13

ELEMENTS OF [s] **FOR** $\lambda = 1/2$

1.4971	0.7496	0	-0.0009	0	-0.0001	0
-0.7777	0	-0.3919	0	0.0031	0	0.0000
0.0040	0.1959	0	-0.1950	0	0.0010	0
0.0061	0	0.1300	0	-0.1273	0	0.0004
0.0005	-0.0008	0	0.0955	0	-0.0947	0
0.0000	0	-0.0004	0	0.0757	0	-0.0755
0.0000	0.0000	0	-0.0002	0	0.0629	0

TABLE 3.14

ELEMENTS OF [S] **FOR** $\lambda = 3/4$

1.7068	0.8512	0	0.0027	0	-0.0005	0
-1.0224	0	-0.5165	0	0.0053	0	0.0000
-0.0088	0.2583	0	-0.2650	0	0.0024	0
0.0107	0	0.1767	0	-0.1723	0	0.0010
0.0021	-0.0013	0	0.1292	0	-0.1273	0
0.0005	0	-0.0010	0	0.1019	0	-0.1011
0.0001	0.0000	0	-0.0005	0	0.0843	0

TABLE 3.15

ELEMENTS OF [S] FOR $\lambda = 1$

of the parameters t, ϵ, and λ may be easily determined. An estimate of the error in any calculation may be made from a "reasonable guess" at the magnitude of the elements which have been neglected in the tabulated matrices. Generally, the error will increase as λ increases.

3.6 Sectional Radial Force and Pitching Moment

For an annular airfoil at zero incidence in a perfect fluid the net forces and moments acting on the airfoil vanish. However, if we consider a section of the duct, then we find that both a radial force, or lift, and a pitching moment are present. The form of the corresponding force and moment coefficients, c_r and c_m respectively, are the same as for a two-dimensional airfoil, or

$$c_r = -\pi(c_0 + \tfrac{1}{2}c_1) \tag{3.18}$$

and

$$c_m = \frac{\pi}{8}(c_1 - c_2) \tag{3.19}$$

where the radial force is positive outwards and the pitching moment is taken about the quarter chord, positive nose-down.

CHAPTER FOUR

NUMERICAL EXAMPLES

4.1 Illustrative Calculation

In order to illustrate the procedure for computing the duct pressure distribution we will work out an example in detail. We take an NACA 0008 airfoil with

$$\epsilon = -\tan 5^\circ$$
$$\lambda = 1/2 \tag{4.1}$$

First, we determine $\{\epsilon\}$. It follows immediately by writing ϵ in the form of Eq. (2.1) and is

$$\{\epsilon\} = \begin{Bmatrix} -0.1750 \\ 0 \\ 0 \\ \cdot \\ \cdot \\ \cdot \end{Bmatrix} \tag{4.2}$$

Next, for the NACA 0008 airfoil $5(t_{max}/c) = 0.4$, and from Table 2.1 we find for $\lambda = 1/2$,

$$\{a\} = \begin{Bmatrix} 0.1188 \\ -0.2521 \\ -0.1238 \\ 0.1951 \\ -0.3248 \\ 0 \\ . \\ . \end{Bmatrix} \tag{4.3}$$

To obtain $\{\epsilon_t\}$ we multiply $\{a\}$ by the appropriate matrix $[Q]$ from Table 2.12 to get

$$\{\epsilon_t\} = \begin{Bmatrix} 0.0005 \\ -0.0356 \\ -0.0116 \\ 0.0009 \\ -0.0005 \\ 0.0002 \\ -0.0002 \end{Bmatrix} \tag{4.4}$$

for the first seven elements.

The two-dimensional Glauert coefficients, or $\{\epsilon\} - \{\epsilon_t\}$, are

$$\{c^{2\text{-}D}\} = \begin{Bmatrix} -0.1755 \\ 0.0356 \\ 0.0116 \\ -0.0009 \\ 0.0005 \\ -0.0002 \\ 0.0002 \end{Bmatrix} \tag{4.5}$$

and so the Glauert coefficients of C are obtained from Eq. (1.20) and Table 1.2 as

$$\{c\} = \begin{Bmatrix} -0.1890 \\ 0.0088 \\ 0.0070 \\ -0.0009 \\ 0.0005 \\ -0.0002 \\ 0.0002 \end{Bmatrix} \tag{4.6}$$

Note that the three-dimensional effect of the duct changes only the first three two-dimensional Glauert coefficients.

With the required Glauert coefficients determined, the expression for the surface pressure coefficient, Eq. (3.17), may be simplified. The first term, $\pm C$, is found from Eqs. (1.19) and (4.6). The contribution of F is obtained from the basic thickness form data in Appendix 1 of Ref. 26. The matrix operations $[T]\{a\}$ and $[S]\{c\}$ are carried out using Tables 3.8 and 3.13 and Eqs. (4.3) and (4.6), yielding

$$[T]\{a\} + [S]\{c\} = \begin{Bmatrix} -0.2195 \\ 0.0945 \\ 0.0036 \\ 0.0007 \\ 0.0000 \\ 0.0000 \\ 0.0000 \end{Bmatrix} \tag{4.7}$$

With this information and $\{\phi\}$ from Eq. (3.12), c_p has been calculated and is plotted in Fig. 4.1. For comparison purposes, the effect of doubling λ while keeping t and ϵ the same has also been computed and is shown in the same figure.

The effect on c_p of varying t is given in Fig. 4.2 for $\epsilon = -\tan 5^\circ$ and $\lambda = 1/2$. Comparison of the results with the previous figure reveals that, for the particular configuration investigated, doubling the chord-to-diameter ratio has a much smaller effect on c_p than a nearly corresponding increase in the thickness ratio.

4.2 Comparison With Previous Results

To assess the accuracy of this new method, we have calculated the velocity and pressure distributions on several annular airfoils to compare with the experimental and theoretical results of previous investigators. The only wind tunnel measurements of pressure, or velocity, distributions published to date which we have found are those of the Bureau Technique Zborowski[11]. In their tests, the circumferential variation of the inner and outer surface pressures on an NACA 66-006, $\lambda = 1$ ring airfoil was measured at several angles of attack. Their data which is appropriate to the present study, i. e., the zero angle of attack results, has been replotted to within ± 0.005 in Fig. 4.3 and compared with the distribution as calculated from Eq. (3.17).

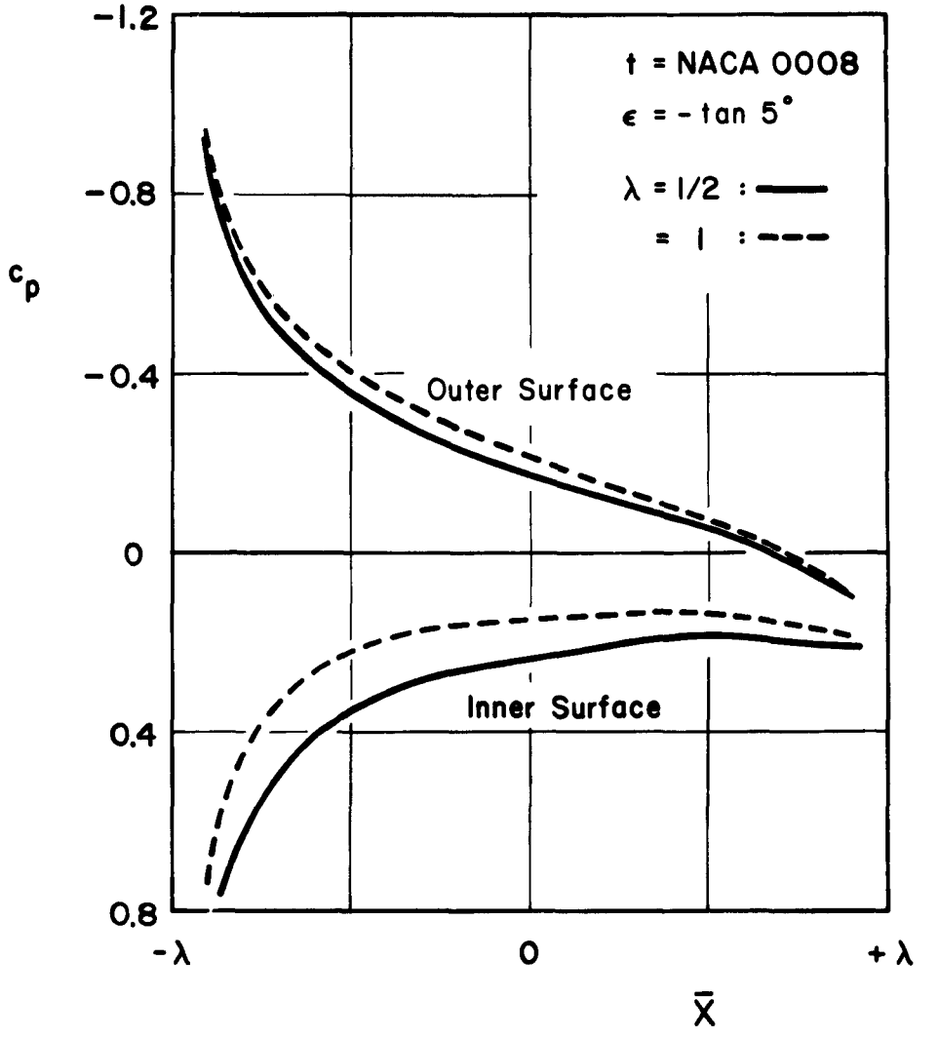

FIGURE 4.1

VARIATION OF PRESSURE DISTRIBUTION WITH DUCT CHORD-TO-DIAMETER RATIO

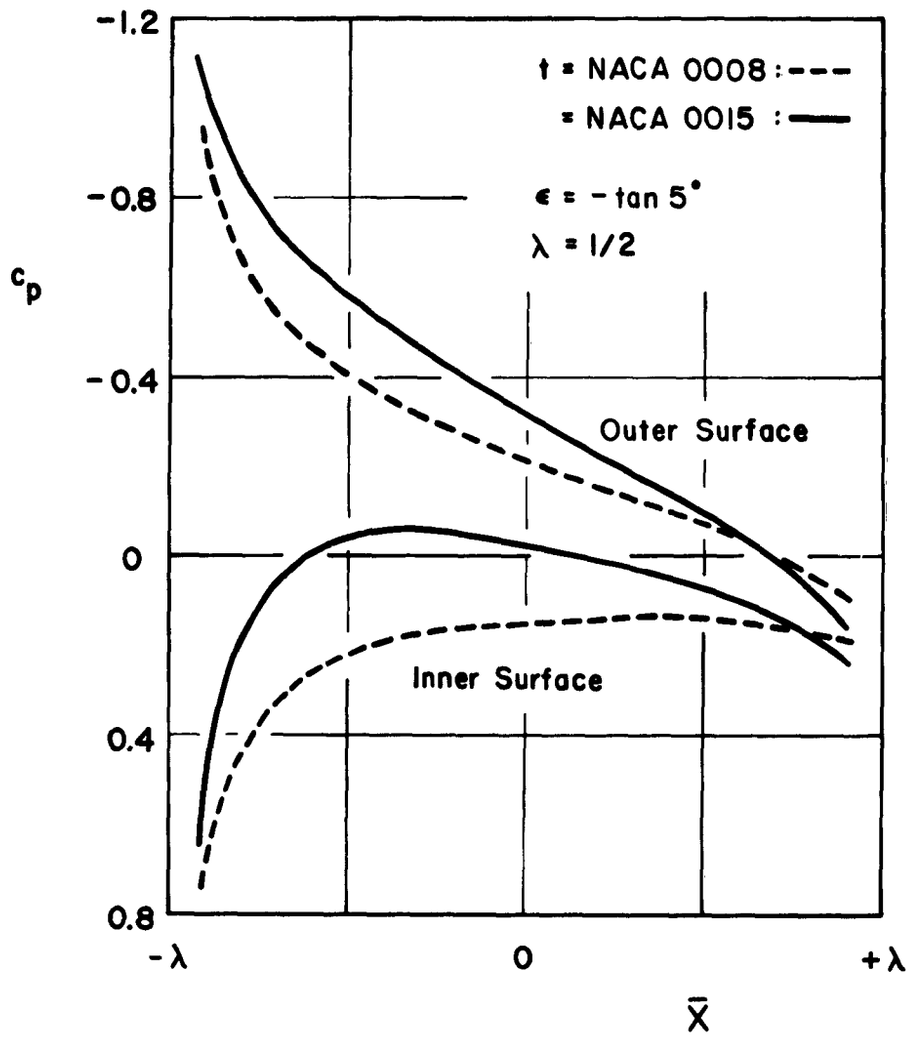

FIGURE 4.2

VARIATION OF PRESSURE DISTRIBUTION WITH DUCT THICKNESS

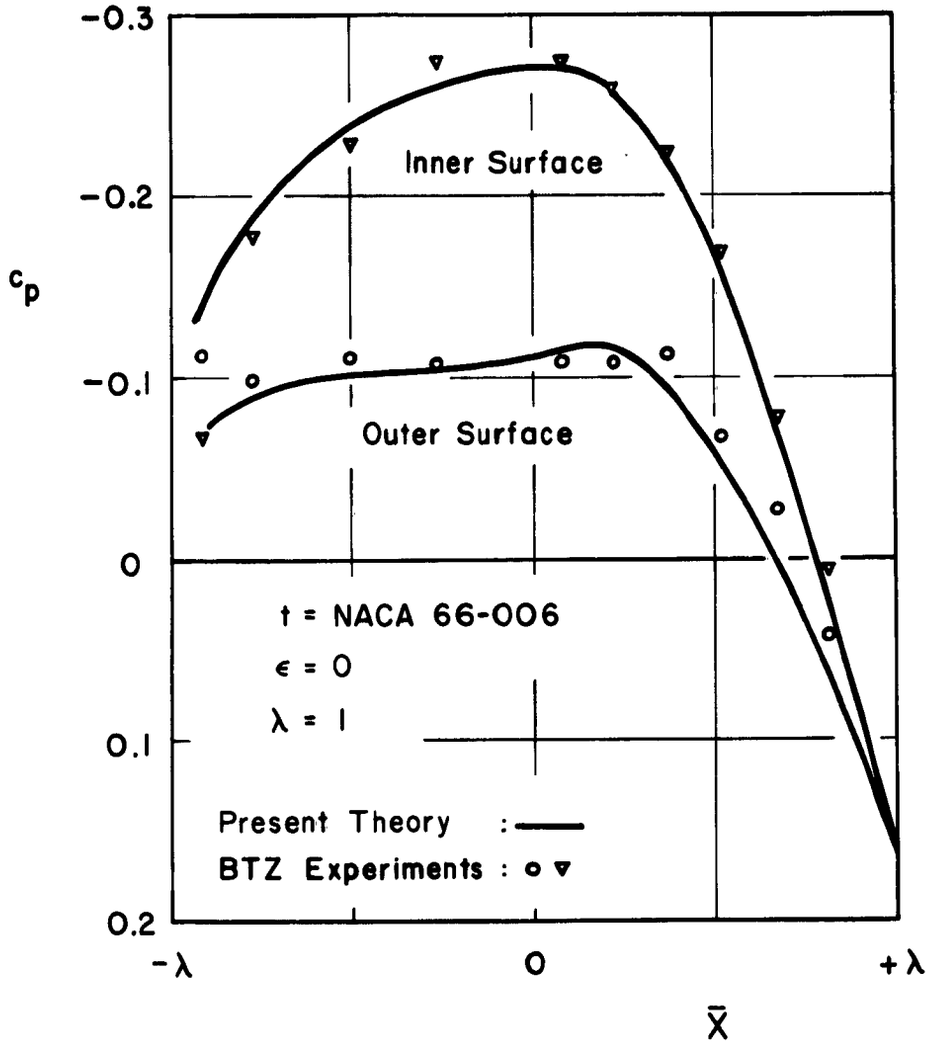

FIGURE 4.3

PRESSURE DISTRIBUTION ON NACA 66-006 ANNULAR AIRFOIL

Except in the immediate vicinity of the leading and trailing edges, the results differ by less than 10%. Better agreement is obtained for the inner surface distribution.

The pressure distribution on a conical ring airfoil of zero thickness as computed from the rheoelectric tank analogy results of Malavard[12] is compared with that of the present theory in Fig. 4.4. Since $\lambda = 2/3$ for this configuration, we have used values of the necessary matrices which were estimated by linear interpolation of the results for $\lambda = 1/2$ and $\lambda = 3/4$. Satisfactory accuracy can be achieved in this manner. In this example, good agreement is obtained for the outer surface distribution only. The discrepancy between the inner surface results has not been resolved.

Bagley, Kirby and Marcer[10] have developed a method for finding the velocity distribution over annular airfoils in incompressible flow. The basis of their work is the approximation of certain integrals by Weber "sum-functions" of the airfoil ordinates[31] and the satisfaction of the resulting set of n linear equations at n points on the airfoil chordline. Comparison with their results for the thickness-induced radial velocity (less the term $\pm \frac{1}{2} f$) on an RAE 101-10% , $\lambda = 1/2$ ring airfoil is shown in Fig. 4.5. Excellent agreement is obtained, the results being indistinguishable except near the trailing edge. Fig. 4.6 compares the induced axial velocities on an RAE 101-10%, $\lambda = 1$ ring airfoil; again, relatively good agreement is obtained.

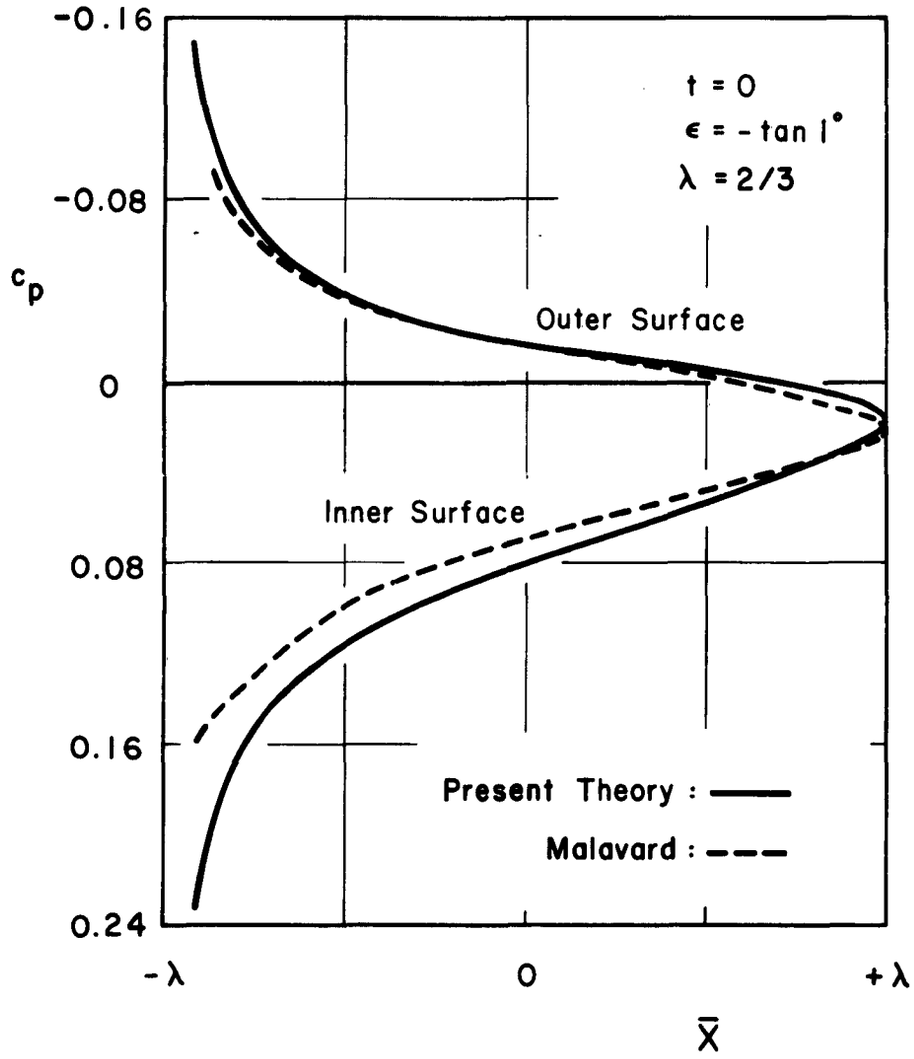

FIGURE 4.4

PRESSURE DISTRIBUTION ON 1° CONICAL RING AIRFOIL

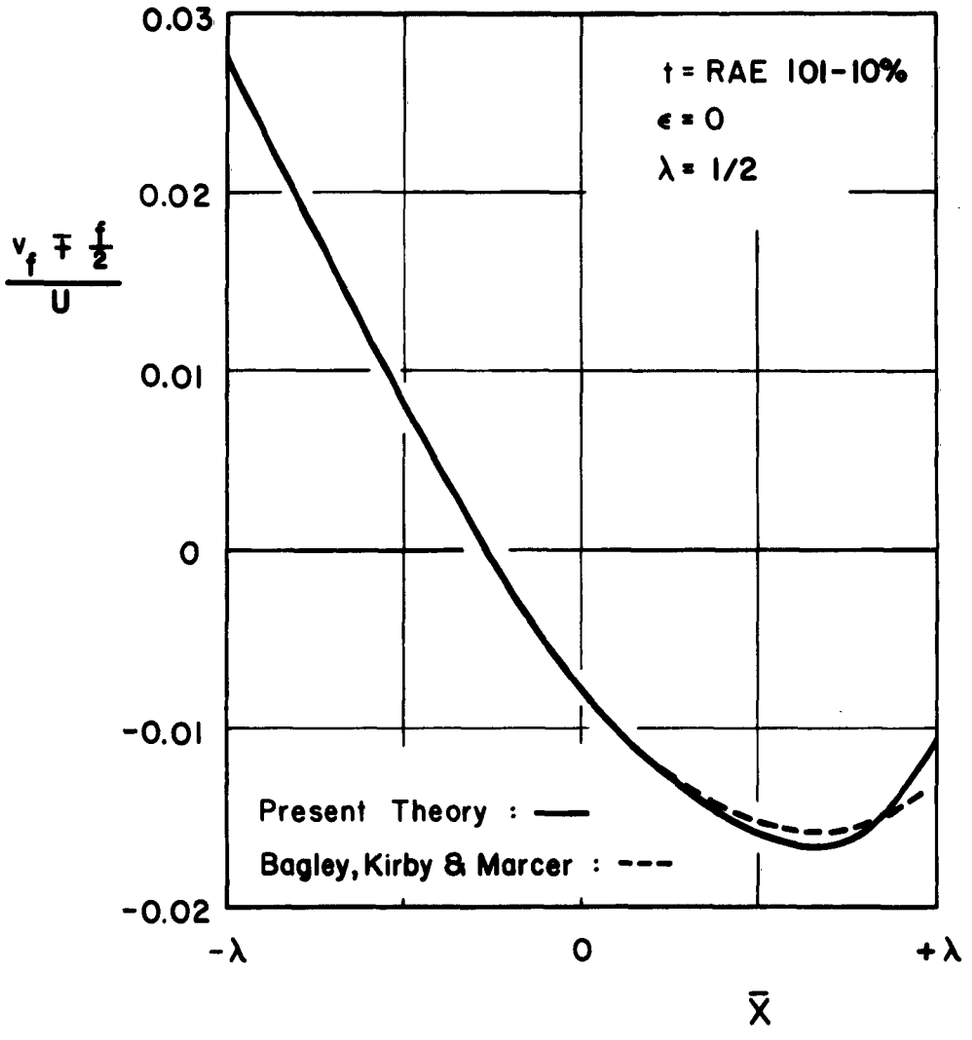

FIGURE 4.5

THICKNESS-INDUCED RADIAL VELOCITY ON RAE 101-10% ANNULAR AIRFOIL

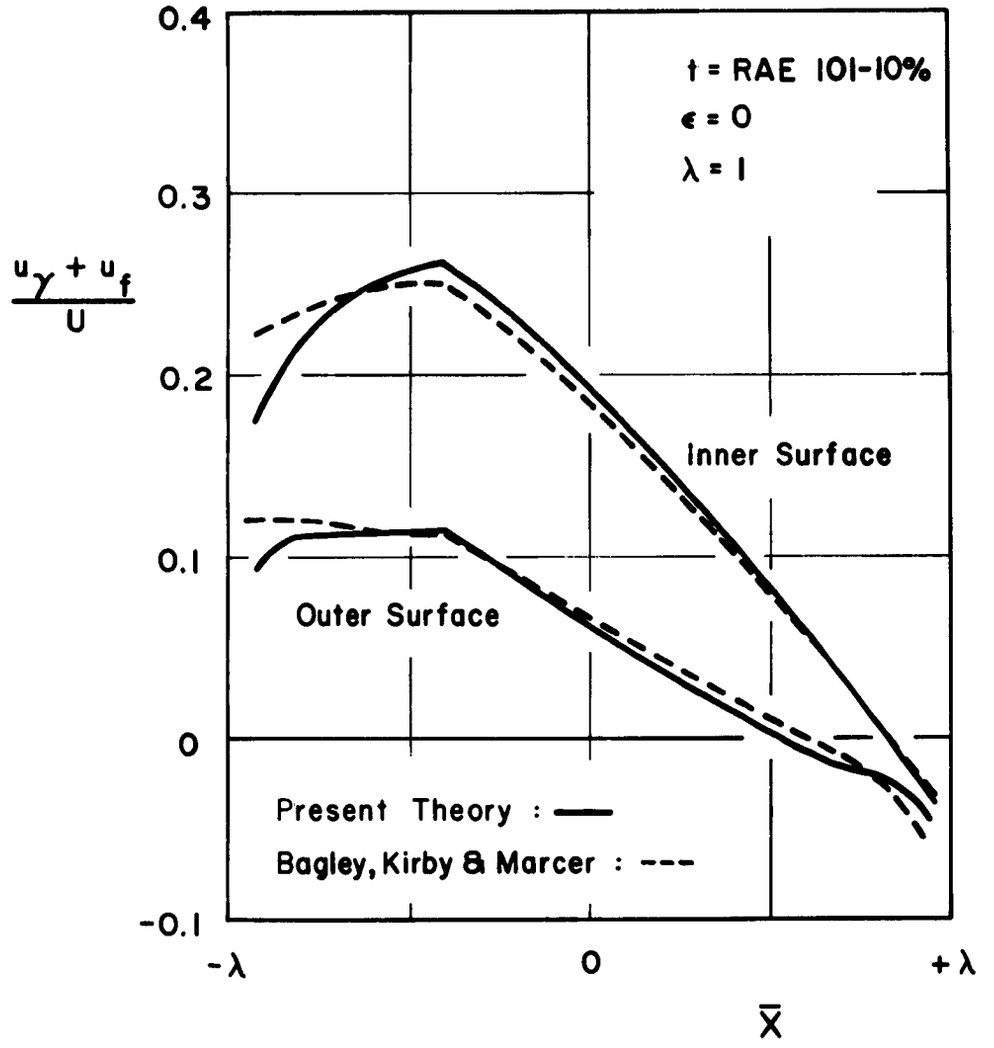

FIGURE 4.6

INDUCED AXIAL VELOCITY ON RAE 101-10% ANNULAR AIRFOIL

We have found that the computation of the pressure distribution at thirteen chordwise stations takes approximately one hour on a desk calculator once $\{\epsilon\}$ and $\{a\}$ are determined. The advance tabulation of $\{\phi\}$ corresponding to these stations proves to be of great assistance in facilitating the numerical work.

CONCLUSIONS

A simple, rapid method for the determination of the linearized surface pressure distribution on streamlined ducted bodies in axial flow has been developed. The pressure coefficient is composed of camber and thickness terms analogous to two-dimensional flow plus an additional term expressed as a matrix operation on the duct sectional properties. Tables of the necessary matrices for four representative duct chord-to-diameter ratios are given; matrices obtained by interpolation from these values can be used for "in-between" chord-to-diameter ratios.

The method is ideally suited for engineering calculations and preliminary design studies and the effects of varying any or all of the thickness and camber distributions and chord-to-diameter ratio may easily be determined.

Comparison of predicted pressure and velocity distributions for several annular airfoils gives good agreement with previous experimental and theoretical results. A typical numerical computation for a given configuration may be done on a desk calculator in about one hour.

The theory may be extended to include the interference effects of a centerbody and/or a propeller as well as duct angle of attack.

REFERENCES

1. Ordway, D. E., Sluyter, M. M., and Sonnerup, B. O. U., Three-Dimensional Theory of Ducted Propellers, THERM, Incorporated, TAR-TR 602, August 1960.

2. Ordway, D. E., and Greenberg, M. D., General Harmonic Solutions for the Ducted Propeller, THERM, Incorporated, TAR-TR 613, August 1961.

3. Ritter, A., and Ordway, D. E., Some Results of Finite-Bladed Ducted-Propeller Theory for VTOL, Aerospace Engineering, Vol. 21, No. 7, July 1962.

4. Dickmann, H. E., Grundlagen zur Theorie ringförmiger Tragflügel (frei umströmte Dusen), Ingenieur-Archiv, Vol. 11, pp. 36-52, 1940.

5. Stewart, H. J., The Aerodynamics of a Ring Airfoil, Quarterly of Applied Mathematics, Vol. II, No. 2, pp. 136-141, 1944.

6. Ribner, H. S., The Ring Airfoil in Nonaxial Flow, Journal of the Aeronautical Sciences, Vol. 14, No. 9, pp. 529-530, September 1957.

7. Küchemann, D., and Weber, J., Aerodynamics of Propulsion, McGraw-Hill Book Co., Inc., 1953.

8. Faure, M. G., Étude Theorétique de l'Aile Annulaire, Tech. et Sci. Aeronautiques, Vol. 6, pg. 293, 1956.

9. Pivko, S., Determination of Velocity and Pressure Distribution along the Surface of Annular Airfoils with Thick Symmetrical Sections, Journal of the Royal Aeronautical Society, Vol. 60, May and July 1956.

10. Bagley, J. A., Kirby, N. B. and Marcer, P. J., A Method of Calculating the Velocity Distribution on Annular Aerofoils in Incompressible Flow, RAE TN No. Aero 2571, June 1958.

11. Ladurner, O., Theoretical Investigation and Examination by Measuring Tests in What a Degree the Economy of Flying Vehicles is Influenced by Pre-Cambered Skeletons of Airfoils Closed in Themselves, Bureau Technique Zborowski, DA-91-508-EUC393, August 1959.

12. Malavard, L. C., Studies of Annular Airfoils by the Electric Analogy, First International Congress in the Aeronautical Sciences, Madrid, Spain, September 1958, Pergamon Press 1959.

13. Weissinger, J., Zur Aerodynamik des Ringflügels in inkompressibler Strömung, Zeitschrift für Flugwissenschaften, Heft 3/4, pp. 141-150, March/April 1956.

14. Weissinger, J., The Ring Airfoil with Deflected Control Surface in Steady Incompressible Flow, AFOSR TR 57-8, Part I, January 1957.

15. Weissinger, J., The Influence of Profile Thickness on Ring Airfoils in Steady Incompressible Flow, AFOSR TR 57-8, Part II, January 1957.

16. Weissinger, J., Ring Airfoil Theory - Problems of Interference and Boundary Layer, AFOSR TN 59-226, January 1959.

17. Weissinger, J., Einige Ergebnisse aus der Theorie des Ringflügels in inkompressibler Strömung, Advances in Aeronautical Sciences, Vol. 2, Pergamon Press, pp. 798-831, 1959.

18. Weissinger, J., Theoretical Investigations on Ring Airfoils, European Office ARDC Report, January 1960.

19. Weissinger, J., Zur Aerodynamik des Ringflügels, IV: Ringflügel mit Zentralkorper, DVL Report 140, Manheim, 1960.

20. Dwight, H. B., Tables of Integrals and other Mathematical Data, The Macmillan Co., New York, Fourth Edition, 1961.

21. Hodgman, C. D., Editor, Mathematical Tables from Handbook of Chemistry and Physics, Chemical Rubber Publishing Co., Cleveland, Ninth Edition, 1952.

22. Sonnerup, B. O. U., Expression as a Legendre Function of an Elliptic Integral Occurring in Wing Theory, THERM, Incorporated, TAR-TN 59-1, November 1959.

23. Ritter, A., and Ordway, D. E., Ducted Propeller and Related Airscrew Studies at TAR, THERM, Incorporated, TAR-TR 614, August 1961.

24. Glauert, H., The Elements of Aerofoil and Airscrew Theory, Cambridge University Press, Second Edition, 1948.

25. von Mises, R., Theory of Flight, Dover Publications, Inc., New York, 1959.

26. Abbott, I. H., and von Doenhoff, A. E., Theory of Wing Sections, Dover Publications, Inc., New York, 1959.

27. Bartholomew, G. E., Numerical Integration Over the Triangle, Mathematical Tables and Other Aids to Computation, pp. 295-298, October 1959.

28. Sluyter, M. M., A Computational Program and Extended Tabulation of Legendre Functions of Second Kind and Half Order, THERM, Incorporated, TAR-TR 601, August 1960.

29. van Dyke, M. D., Second-Order Subsonic Airfoil Theory Including Edge Effects, NACA Report 1274, 1956.

30. Thwaites, B., Editor, Incompressible Aerodynamics, Oxford at the Clarendon Press, 1960.

31. Weber, J., The Calculation of the Pressure Distribution over the Surface of Two-Dimensional and Swept Wings with Symmetrical Airfoil Sections, RAE Report Aero 2497, July 1953.

32. Churchill, R. V., Introduction to Complex Variables and Applications, McGraw-Hill Book Co., Inc., New York, 1948.

APPENDIX

Derivations of certain integrals referred to in the main portion of the text are given here:

$$\int_0^{\pi} \cos n\phi \, \ell n(1+\cos\phi) \, d\phi \quad , \quad n \geq 1$$

We integrate by parts with $u = \ell n(1+\cos\phi)$ and $dv = \cos n\phi \, d\phi$. Upon carrying this out, we find that the contribution of uv vanishes and we are left with

$$\frac{1}{n} \int_0^{\pi} \frac{\sin\phi \sin n\phi}{1+\cos\phi} \, d\phi$$

This is evaluated in turn for each n by expanding $\sin n\phi$ in powers of $\sin\phi$, removing the factor $\sin\phi$, and dividing $(1+\cos\phi)$ into $\sin^2\phi = (1+\cos\phi)(1-\cos\phi)$. The integral is then readily reduced and the results generalized to give

$$\int_0^{\pi} \cos n\phi \, \ell n(1+\cos\phi) \, d\phi = \frac{(-1)^{n+1} \pi}{n} \quad , \quad n \geq 1 \qquad \text{(A.1)}$$

$$\int_0^{\pi} \sin\phi \, \ell n \, \frac{1+\sin\phi}{1-\sin\phi} \, d\phi$$

We integrate by parts with $u = \ell n \, \frac{1+\sin\phi}{1-\sin\phi}$ and $dv = \sin\phi \, d\phi$. The contribution uv vanishes and, after trigonometric reduction, $v \, du$ is simply 2 , so that

$$\int_0^{\pi} \sin\phi \, \ell n \, \frac{1+\sin\phi}{1-\sin\phi} \, d\phi = 2\pi \qquad \text{(A.2)}$$

$$\int_0^{\pi} \cos^{2n}\phi \, \sin\phi \, \ell n \, \frac{1+\sin\phi}{1-\sin\phi} \, d\phi \quad , \quad n \geq 1$$

We integrate by parts with $u = \ell n \, \frac{1+\sin\phi}{1-\sin\phi}$ and $dv = \cos^{2n}\phi \, \sin\phi \, d\phi$. Then uv vanishes and we are left with

$$\frac{2}{2n+1} \int_0^{\pi} \cos^{2n}\phi \, d\phi$$

Changing to a period of $\pi/2$, we can integrate this in turn by means of Formula 858.44 of Ref. 20 to obtain

$$\int_0^{\pi} \cos^{2n}\phi \, \sin\phi \, \ell n \, \frac{1+\sin\phi}{1-\sin\phi} \, d\phi = \frac{2\pi}{2n+1} \, \frac{1 \cdot 3 \cdot 5 \ldots (2n-1)}{2 \cdot 4 \cdot 6 \ldots \quad 2n} \quad , \quad n \geq 1$$

(A.3)

$$\int_0^{\pi} \ln(\cos\varphi - \cos\phi)^2 \, d\varphi$$

We integrate by parts with $u = \ln(\cos\varphi - \cos\phi)^2$ and $dv = d\varphi$ to get

$$\pi \ln(1+\cos\phi)^2 + 2 \int_0^{\pi} \frac{\varphi \sin\varphi}{\cos\varphi - \cos\phi} \, d\varphi$$

This integral is somewhat similar in form to the Glauert integral and can be evaluated by complex contour integration. Making the substitution $z = e^{i\varphi}$, we study a related integral of the form

$$\int_C i \frac{(z-z^{-1})(\ln z)}{(z-e^{i\phi})(z-e^{-i\phi})} \, dz$$

where C is the closed curve composed of C_1, C_2, C_3, the indentations at $\pm\phi$, L_1, C_4, and L_2; viz.,

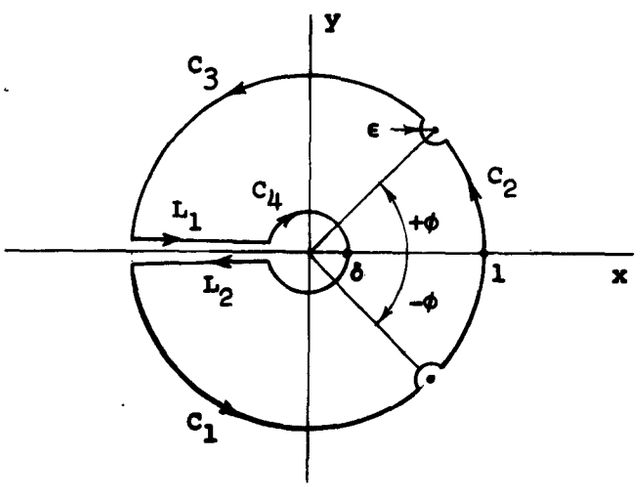

The integrand is analytic inside the region bounded by C and thus, using the residue theorem[32] of complex variables, we have

$$\int_{C_1} + \int_{e^{-i\phi}} + \int_{C_2} + \int_{e^{i\phi}} + \int_{C_3} + \int_{L_1} + \int_{C_4} + \int_{L_2} = 0$$

On the identation at $+\phi$, $z = e^{i\phi} + \epsilon e^{i\alpha}$ where α turns through an angle of $-\pi$. The contribution here is evaluated taking the limit as $\epsilon \to 0$. At the lower indentation, $-\phi$, $z = e^{-i\phi} + \epsilon^{i\alpha}$, and after passing to the limit $\epsilon \to 0$, we find that the contribution here exactly cancels that at $+\phi$. On L_1, $z = re^{i\pi}$ while on L_2, $z = re^{-i\pi}$. The contributions of L_1, and L_2 are combined and simplified to yield

$$\int_{L_1} + \int_{L_2} = 2\pi \int_{\delta}^{1} \frac{(r-r^{-1})\, dr}{r^2 + 2r\cos\phi + 1}$$

$$= \pi \ln 4(1+\cos\phi)^2 + 2\pi \ln \delta$$

On C_4, $z = \delta e^{i\theta}$, $-\pi \leq \theta \leq \pi$, and, after simplification, we find that

$$\int_{C_4} = -2\pi \ln \delta$$

Collecting these results, we have

$$\int_{C_1+C_2+C_3} = -\pi \ln 4(1+\cos\phi)^2$$

where $C_1 + C_2 + C_3$ is now the unit circle, so that

$$\int_{-\pi}^{\pi} \frac{\varphi \sin\varphi \, d\varphi}{\cos\varphi - \cos\phi} = -\pi \ln 4(1+\cos\phi)^2 \qquad (A.4)$$

and thus, since $\varphi \sin\varphi/\cos\varphi - \cos\phi$ is even in φ,

$$\int_{0}^{\pi} \ln(\cos\varphi - \cos\phi)^2 \, d\varphi = -\pi \ln 4 \qquad (A.5)$$

$$\int_{0}^{\pi} \cos n\varphi \ln(\cos\varphi - \cos\phi)^2 \, d\varphi \quad , \quad n \geq 1$$

We integrate by parts with $u = \ln(\cos\varphi - \cos\phi)^2$ and $dv = \cos n\varphi \, d\varphi$; uv vanishes and we are left with

$$\frac{2}{n} \int_{0}^{\pi} \frac{\sin\varphi \sin n\varphi}{\cos\varphi - \cos\phi} \, d\varphi$$

Replacing $\sin\varphi \sin n\varphi$ by its equivalent sum of two cosines, we use the Glauert integral[24] or

$$\int_{0}^{\pi} \frac{\cos p\varphi}{\cos\varphi - \cos\phi} \, d\varphi = \pi \frac{\sin p\varphi}{\sin\varphi} \quad , \quad p \geq 0$$

and reduce the results to

$$\int_{0}^{\pi} \cos n\varphi \ln(\cos\varphi - \cos\phi)^2 \, d\varphi = -\frac{2\pi}{n} \cos n\phi \quad , \quad n \geq 1 \qquad (A.6)$$

$$\int_0^{\pi} \sin \nu\varphi \cos q\varphi \sin\varphi \, d\varphi$$

We decompose the integrand into the sum of four cosines by Formula 402.05 of Ref. 20, or

$$4 \sin \nu\varphi \cos q\varphi \sin\varphi = [\cos(q+1-\nu)\varphi + \cos(q+1+\nu)\varphi - \cos(q-1+\nu)\varphi - \cos(q-1-\nu)\varphi]$$

The subsequent integrations are easily carried out, giving

$$\int_0^{\pi} \sin \nu\varphi \cos q\varphi \sin\varphi \, d\varphi = \frac{\pi}{2}, \quad \nu = 1 \ \& \ q = 0$$

$$= \pm \frac{\pi}{4}, \quad \nu = q \mp 1 \ \& \ q \geq 1 \qquad (A.7)$$